Irisin alleviates oxidative stress and osteoblast apoptosis in glucocorticoid-induced rat osteonecrosis of the femoral head via the integrin αVβ5/Bach1/Nrf2 signaling pathway

XIN ZHANG[1], YUANKAI ZHANG[2], YAN ZHAO[2], KEKE SONG[3], XIAOFEI LIU[4], KAI NAN[5] and LIHONG FAN[2,6]

[1]Department of Orthopedics, Tangdu Hospital, The Fourth Military Medical University, Xi'an, Shaanxi 710038, P.R. China; [2]Department of Orthopedics, The Second Affiliated Hospital of Xi'an Jiaotong University, Xi'an, Shaanxi 710004, P.R. China; [3]Department of Anesthesiology, The First Affiliated Hospital of Xi'an Jiaotong University, Xi'an, Shaanxi 710061, P.R. China; [4]Center for Regenerative and Reconstructive Medicine, Med-X Institute, The First Affiliated Hospital of Xi'an Jiaotong University, Xi'an, Shaanxi 710061, P.R. China; [5]Department of Joint Surgery, Honghui Hospital, Xi'an Jiaotong University, Xi'an, Shaanxi 710054, P.R. China; [6]Department of Orthopedics, The Affiliated Sanya Central Hospital of Hainan University, Sanya, Hainan 572000, P.R. China

Received May 11, 2026; Accepted October 7, 2026

DOI: 10.3892/ijmm.2026.6050

Abstract. Glucocorticoid (GC)-induced osteonecrosis of the femoral head (ONFH) is associated with oxidative stress and osteoblast apoptosis. Irisin, the cleaved form of fibronectin type III domain-containing protein 5, attenuates oxidative stress and apoptosis in numerous types of cells, including osteoblasts, osteocytes and cardiomyocytes. The present study aimed to investigate the role of irisin and the mechanism behind GC-induced ONFH *in vivo*, as well as oxidative stress and osteoblast apoptosis *in vitro*. In the present study, GC-induced ONFH was established in rats by intramuscular injection of methylprednisolone, with irisin administered by intraperitoneal injection; the FHs were then assessed by micro-CT, histology, immunohistochemistry and TUNEL staining. *In vitro*, murine osteoblastic MC3T3-E1 cells were treated with dexamethasone (DEX), and oxidative stress, apoptosis and Nrf2 signaling were evaluated by dihydroethidium/JC-1 staining, flow cytometry, reverse transcription-quantitative PCR and western blotting. Irisin prevented the development of GC-induced ONFH in rats, and alleviated oxidative stress and apoptosis in DEX-treated osteoblasts. To determine the underlying mechanisms by which irisin exerted beneficial effects on DEX-treated osteoblasts, the present study investigated Nrf2 signaling cascades. Irisin induced Nrf2 signaling cascade activation in MC3T3-E1 cells and Nrf2 silencing by targeted short hairpin RNA reversed the beneficial effects of irisin on DEX-treated osteoblasts. Further mechanistic analysis revealed that irisin physically interacted with integrin (ITG) αVβ5 on osteoblasts, activating Erk1 signaling. This activation promoted nuclear export of Bach1, a competitive suppressor of Nrf2, thereby relieving Bach1-mediated suppression of antioxidant response elements. Consequently, irisin enhanced Nrf2 nuclear accumulation and upregulated its target genes [heme oxygenase, NAD(P)H quinone oxidoreductase 1, glutamate-cysteine ligase catalytic subunit], reducing reactive oxygen species and mitochondrial membrane potential loss. Pharmacological inhibition of ITG αVβ5 or Erk1/2 abolished irisin-induced Bach1 export, Nrf2 activation and cytoprotective effects. Collectively, the present study indicated that irisin may mitigate GC-induced ONFH and osteoblast apoptosis via the ITG αVβ5/Bach1/Nrf2 signaling pathway, highlighting its therapeutic potential.

Correspondence to: Dr Xin Zhang, Department of Orthopedics, Tangdu Hospital, The Fourth Military Medical University, 569 Xinsi Road, Xi'an, Shaanxi 710038, P.R. China
E-mail: zhxin07@qq.com

Professor Lihong Fan, Department of Orthopedics, The Affiliated Sanya Central Hospital of Hainan University, 1154 Jiefang 4th Road, Sanya, Hainan 572000, P.R. China
E-mail: drfan2140@xjtu.edu.cn

Key words: glucocorticoid, osteonecrosis of the femoral head, irisin, Bach1, Nrf2

Introduction

Glucocorticoids (GCs) are used as part of the therapeutic regimen for certain types of autoimmune and allergic diseases due to their immunosuppressive and anti-inflammatory effects. However, their prolonged and excessive use can lead to serious adverse effects, such as GC-induced osteonecrosis of the femoral head (ONFH). This condition affects 9-40% of patients receiving long-term GC therapy and is the most common cause of non-traumatic ON (1,2). ONFH is characterized by progressive joint pain and dysfunction, which may require hip replacement surgery (3). Despite the association between GCs and ONFH, the underlying pathophysiological mechanisms remain elusive.

GC-induced excess reactive oxygen species (ROS) generation and accumulation, as well as subsequent oxidative stress and apoptosis in osteoblasts, serve pivotal roles in the development of ONFH (4-6). GCs not only stimulate ROS generation

by activating the NOX isozyme family proteins, but also impair ROS scavenging by inhibiting antioxidant enzymes (6). Excessive ROS can oxidize biological macromolecules, impede protein function and cause cell death (7). Moreover, ROS can induce apoptosis via both the death receptor- and mitochondria-mediated pathways (7). Conversely, blocking ROS and oxidative stress partially prevents GC-induced ONFH and apoptosis (8,9).

Nrf2 is a key component participating in the endogenous antioxidant mechanism; under physiological conditions, it exists in the cytoplasm, binding to Kelch-like ECH-associated protein 1 (Keap1), with rapid degradation by the ubiquitin-proteasome system maintaining relatively low Nrf2 levels (10,11). Under excessive oxidative stress, Nrf2 plays an antioxidant role by dissociating from Keap1, translocating from the cytoplasm to the nucleus and binding to antioxidant response elements (AREs) to initiate the transcription and expression of antioxidative gene [including heme oxygenase (HO)-1 and NAD(P)H quinone oxidoreductase (NQO)1] (8,10,12). Notably, Nrf2 activation may attenuate GC-induced oxidative stress injury and subsequent osteoblast apoptosis (6).

Bach1 is a heme-sensitive transcription factor belonging to the CNC basic leucine zipper family, which serves as a critical regulator of oxidative stress responses by competitively binding to AREs in target gene promoters (13). Under physiological conditions, Bach1 dimerizes with small Maf proteins to suppress the expression of antioxidative genes, thereby amplifying cell susceptibility to oxidative damage (14,15). The functional interplay between Bach1 and Nrf2 is a key axis in redox homeostasis. While Nrf2 activates ARE-driven transcription to enhance antioxidant defenses, Bach1 antagonizes this process by displacing Nrf2 from ARE sites, thereby suppressing the expression of genes (15,16). This competitive inhibition establishes a dynamic equilibrium wherein cell redox status dictates the Bach1/Nrf2 ratio, ultimately determining oxidative injury outcomes (13). Thus, modulating Bach1 activity offers a promising therapeutic strategy for mitigating oxidative stress.

Irisin is a peptide hormone derived from the cleavage of fibronectin type III domain-containing protein 5 (FNDC5) in skeletal muscle and myocardium during exercise. Since its discovery in 2012, irisin has attracted attention for its role in inducing the browning of white adipose tissue, and its beneficial effects on metabolic disorders such as obesity and insulin resistance, and on cardiovascular disorders such as atherosclerosis and heart failure (17,18). Irisin is also involved in bone metabolism, and modulates the proliferation, differentiation and apoptosis of osteocytes, osteoblasts and osteoclasts (19-25). Moreover, exogenous irisin has been shown to inhibit the apoptosis of osteoblasts and osteocytes (19,21,22). Irisin decreases ROS production and attenuates oxidative stress and apoptosis in different cell types, including osteoblasts, cardiomyocytes and endothelial cells (19,26,27). Furthermore, irisin treatment can increase the nuclear levels of Nrf2 in various cells (19,28,29).

It was hypothesized that irisin may prevent GC-induced ONFH, and protect osteoblasts from oxidative stress and apoptosis through a Nrf2-dependent mechanism. The present study aimed to investigate the function and mechanism of irisin in GC-induced ONFH and to evaluate its therapeutic potential for this condition. The findings of the present study may provide novel information regarding the pathogenesis and treatment of GC-induced ONFH.

Materials and methods

Animal experiments. Animal experimental and care procedures were approved by the Laboratory Animal Ethics Committee of Xi'an Jiaotong University (Xi'an, China; approval no. XJTUAE2025-1953) and were performed following the Animal Research: Reporting of *In Vivo* Experiments guidelines (30) and National Research Council's Guide for the Care and Use of Laboratory Animals guidelines (31). In total, 60 male Sprague-Dawley rats (age, 10 weeks; weight, 280-360 g) were obtained from the Experimental Animal Center of Xi'an Jiaotong University. Rats were housed under controlled conditions (22±2˚C, 50±10% relative humidity, 12-h light/dark cycle) with *ad libitum* access to standard chow and water. All animals were acclimated for 7 days prior to the experiments. Rats were randomly assigned into three groups (n=20/group) using a random number table, as follows: i) Control, rats received an equal volume of saline by intramuscular injection; ii) Model, rats received methylprednisolone (MPS; 20 mg/kg/day; Pfizer, Inc.) by intramuscular injection for the first 3 days of each week for 3 weeks; iii) Irisin, rats received the same MPS regimen and, immediately after each MPS injection, irisin (100 μg/kg; cat. no. 067-29A; Phoenix Pharmaceuticals, Inc.) by intraperitoneal injection. Rats in the Control and Model groups received an equal volume of saline. All animals were monitored daily throughout the experimental period for general condition, body weight, and food and water intake. Pre-defined humane endpoints were as follows: Loss of ≥20% of initial body weight; sustained loss of appetite or inability to access food or water for >24 h; severe lethargy, hunched posture or ruffled fur; inability to right itself or to ambulate; labored or rapid respiration; persistent hypothermia (rectal temperature <35˚C); or any other sign of severe, unrelieved pain or distress. Any animal meeting one or more of these criteria would have been euthanized immediately by intraperitoneal injection of sodium pentobarbital (200 mg/kg body weight), followed by cervical dislocation to confirm death. No animal reached any of the humane endpoints during the present study. During the experimental period, two rats in the Control group died unexpectedly. Although these animals received only saline injection without MPS, their deaths may be attributable to complications associated with the injection procedure (cervical spine injury during handling or individual sensitivity to the stress of repeated intraperitoneal injection). In the Model group, five rats died before the endpoint, likely due to MPS injection-associated complications such as gastrointestinal bleeding, severe infection or multi-organ failure, which are known adverse effects of high-dose GC administration (32). In the Irisin group, four rats died, potentially due to similar MPS-related toxicities, as irisin was administered concurrently and may not have fully rescued the acute systemic toxicity of MPS. These 11 rats were all found dead during routine daily inspections and none of them had exhibited any of the pre-defined humane endpoints prior to death. Ultimately, 18 rats in the Control, 15 in the Model and 16 in the Irisin group were included in the analysis.

Sample size was calculated for pairwise comparisons using the formula for two-sample proportions as follows:

$$n = \frac{(Z_{\alpha/2} + Z_{\beta})^2 \times [p_1(1 - p_1) + p_2(1 - p_2)]}{(p_1 - p_2)^2}$$

where n is the required sample size per group; $Z_{\alpha/2}$ is the critical value of the standard normal distribution corresponding to the Bonferroni-adjusted two-tailed significance level; Z_{β} is the standard normal value corresponding to 80% power; and p_1 and p_2 are the expected proportions of ONFH incidence in the two groups being compared.

To account for multiple comparisons, the significance level was adjusted using Bonferroni's correction ($\alpha'=0.05/3\approx0.0167$), giving a two-tailed critical value of $Z_{\alpha/2}=2.39$. Power was set at 0.80 ($Z_{\beta}=0.84$). Based on pilot experiments, the expected ONFH incidence was ~0% in the Control group, 80% in the Model group and 20% in the Irisin group. The largest required sample size was obtained for the comparison between the Model and Irisin groups ($p_1=0.80$, $p_2=0.20$). According to the aforementioned formula, a minimum of 10 rats/group was required. Considering potential attrition, 20 rats were initially assigned to each group.

All histological and micro-computed tomography (CT) analyses were performed by investigators blinded to group allocation. The GC-induced ONFH model was established according to a previous study (33). For the ONFH model induction, rats received daily intramuscular injection with MPS (20 mg/kg/day; Pfizer, Inc.) for the first 3 days of each week for 3 weeks, while the rats in the Control group received equivalent saline. After each MPS injection, the Irisin group was administered with irisin (0.1 ml; 100 μg/kg) and the remaining groups received an equal volume of saline. The dose of irisin used in the present study has been used in previous studies (25,34).

All rats were euthanized by intraperitoneal injection of sodium pentobarbital at a dose of 200 mg/kg body weight 3 weeks after the last MPS injection, at the end of week 6. Animals were placed in a quiet area and monitored until complete cessation of vital signs. Death was confirmed by the absence of chest wall movement, lack of palpable heartbeat, absence of corneal and toe pinch reflexes and fixed/dilated pupils, sustained for ≥5 min. Subsequently, a secondary physical method (cervical dislocation) was performed to ensure death before tissue harvesting. All procedures were conducted in accordance with the approved animal care protocol and AVMA Guidelines for the Euthanasia of Animals (2020 Edition) (35). Micro-CT, immunohistochemical (IHC) and histomorphological analyses were performed on the collected FH of sacrificed rats at the end of week 6.

Micro-CT scans. Rat FHs were collected, preserved in 4% paraformaldehyde at room temperature for 48 h, and scanned with high-resolution micro-CT (Y. Cheetah) at 9 μm/pixel resolution. DataViewer software (version 1.5.6.2, Bruker Corporation) was used to reconstruct the three-dimensional image of representative samples. Within the subchondral region of interest, the trabecular (Tb) bone parameters were calculated, including bone volume/total volume fraction (BV/TV), Tb separation (Tb.Sp) and thickness (Tb.Th) (36).

Hematoxylin and eosin (H&E) staining. The rat FHs were fixed with 4% paraformaldehyde at room temperature for 48 h. After decalcification in 10% EDTA (pH 7.4) at room temperature for 4 weeks (the solution being refreshed every 3 days), the specimens were dehydrated through a graded ethanol series and embedded in paraffin. The specimens were sectioned to a thickness of 5 μm, stained with hematoxylin for 5 min and eosin for 2 min at room temperature, and examined under a light microscope (Olympus Corporation). All histological and immunohistochemical procedures, including H&E, IHC and TUNEL staining, were performed on separate serial sections (5 μm) cut from the same paraffin-embedded FH blocks. Dihydroethidium (DHE) staining was performed on separate fresh-frozen sections (5 μm) prepared from the same FHs.

DHE staining. Fresh-frozen FH sections (5 μm) were prepared at -20˚C and incubated with DHE (10 μM; cat. no. D7008; Sigma-Aldrich; Merck KGaA) for 30 min at 37˚C in the dark. The sections were then rinsed three times with PBS and the nuclei were counterstained with DAPI (1:1,000) for 5 min at room temperature. Images were captured under a fluorescence microscope (BX53; Olympus Corporation) using the red channel (excitation, ~535 nm; emission, ~610 nm), and the fluorescence intensity in the subchondral bone was quantified using ImageJ (version 1.53t; National Institutes of Health) by two researchers blinded to the treatment groups.

IHC staining. To detect apoptosis and oxidative stress-associated protein expression in rat FH tissue, IHC staining was performed. The FH tissues were fixed in 4% paraformaldehyde at room temperature for 48 h, decalcified in 10% EDTA (pH 7.4) at room temperature for 4 weeks, dehydrated in a descending alcohol series, cleared in xylene and embedded in paraffin. Sections (5 μm) were deparaffinized in xylene, rehydrated through a descending ethanol series, and subjected to antigen retrieval in 10 mM citrate buffer (pH 6.0) at 95-100˚C for 15 min. After which, endogenous peroxidase was quenched with 3% hydrogen peroxide for 10 min and the sections were blocked with 10% normal goat serum (cat. no. SL038; Beijing Solarbio Science & Technology Co., Ltd.) for 30 min at 37˚C. Sections were then incubated overnight at 4˚C with primary antibodies against total caspase-3, cleaved caspase-3, HO-1 and NQO1, followed by incubation with HRP-conjugated goat anti-rabbit IgG for 1 h at room temperature. Sections were treated with DAB for 10 min; brown staining was considered positive expression, and the sections were counterstained with hematoxylin for 5 min at room temperature. Images were captured using a light microscope (BX53; Olympus Corporation). The numbers of HO-1-, NQO1-, total caspase-3- and cleaved caspase-3-positive cells were counted in five randomly selected fields of view per section by two researchers blinded to the experimental groups, and were expressed as the number of positive cells per field.

TUNEL staining. Apoptosis in rat FH sections and in MC3T3-E1 cells was detected by TUNEL staining using the *In Situ* Cell Death Detection kit (Fluorescein; cat. no. 11684795910; Roche Diagnostics GmbH) for tissue sections and the In Situ Cell Death Detection kit (TMR red; cat. no. 12156792910; Roche Diagnostics GmbH) for cultured cells, in accordance with the manufacturer's protocols. Adjacent serial sections (5 μm) obtained from the same paraffin-embedded FH blocks used

for H&E and IHC staining were deparaffinized in xylene and rehydrated, permeabilized with proteinase K (20 μg/ml) for 15 min at room temperature, rinsed three times with PBS and incubated with 50 μl TUNEL reaction mixture for 60 min at 37˚C in the dark. MC3T3-E1 cells grown on coverslips were fixed in 4% paraformaldehyde for 15 min at room temperature, permeabilized with 0.1% Triton X-100 for 10 min and incubated with 50 μl TUNEL reaction mixture under the same conditions. In both cases, nuclei were counterstained with DAPI (1:1,000) for 5 min at room temperature, rinsed three times with PBS and mounted with an anti-fade mounting medium; TUNEL-positive nuclei appeared green in tissue sections and red in cultured cells, whereas all nuclei were stained blue with DAPI. Sections and coverslips were examined under a fluorescence microscope (BX53; Olympus Corporation). For tissue sections, five randomly selected fields of view per section were analyzed, and the apoptotic rate was calculated as the percentage of TUNEL-positive cells among DAPI-stained cells by two researchers who were blinded to the experimental groups. For MC3T3-E1 cells, five randomly selected fields of view per sample were analyzed and the percentage of TUNEL-positive cells among DAPI-stained cells was calculated by two researchers blinded to the treatment groups (saline control, DEX 10 μM and DEX 10 μM plus irisin 100 ng/ml).

Western blot analysis. Western blotting of rat FH tissue and MC3T3-E1 cells was performed using a unified protocol. FH tissue was harvested, washed with ice-cold PBS, and homogenized in RIPA lysis buffer (Beyotime Biotechnology) containing protease and phosphatase inhibitors (Roche Diagnostics GmbH) using a tissue grinder. MC3T3-E1 cells treated with DEX (10 μM) with or without irisin (100 ng/ml) for 48 h were lysed in the same RIPA buffer. Lysates were centrifuged at 12,000 x g for 15 min at 4˚C and the supernatants were collected. Protein concentrations were quantified using a BCA Protein Assay kit (Beyotime Biotechnology) according to the manufacturer's instructions. Equal amounts of protein (30 μg/lane) were separated by 10% SDS-PAGE and transferred onto PVDF membranes (MilliporeSigma). The membranes were blocked with 5% non-fat dried milk in TBS-0.1% Tween-20 (TBST) for 1 h at room temperature, and then incubated overnight at 4˚C with the following primary antibodies against HO-1, NQO1, SOD1, BCL-2, BAX, cleaved caspase-3, total caspase-3 and GAPDH. After three washes with TBST, the membranes were incubated with HRP-conjugated goat anti-rabbit or anti-mouse IgG secondary antibodies for 1 h at room temperature. Protein bands were visualized using an enhanced chemiluminescence (ECL) reagent (Tiangen Biotech Co., Ltd.) and the blots were semi-quantified using ImageJ. GAPDH served as the loading control. Comprehensive antibody information (dilution, cat. no. and supplier) is provided in Table SI.

Cell culture. Murine osteoblastic MC3T3-E1 cells obtained from the China Center for Type Culture Collection were cultured at 37˚C in 5% humidified CO_2 in α-MEM (Sigma-Aldrich; Merck KGaA) supplemented with 10% FBS (cat. no. F2442; Sigma-Aldrich; Merck KGaA) and 100 U/ml penicillin/streptomycin for 3 days. To identify the roles of irisin on dexamethasone (DEX)-treated MC3T3-E1 cells, cells were treated with DEX (10 μM; cat. no. D4902; Sigma-Aldrich; Merck KGaA) alone or in combination with irisin at 37˚C in a humidified atmosphere of 5% CO_2. Irisin was used at a low dose (10 ng/ml) or a high dose (100 ng/ml), unless otherwise indicated; the dose-response was first established across a range of 1, 10 and 100 ng/ml in the Cell Counting Kit (CCK)-8 assay. The duration of treatment was assay-dependent: 24 h for DHE and JC-1 staining, 48 h for flow cytometric analysis and western blotting, and 72 h for the CCK-8 and lactate dehydrogenase (LDH) assays.

Cell proliferation and toxicity assay. MC3T3-E1 cell proliferation was assessed using a CCK-8 kit (Dojindo Laboratories, Inc.). The cells were seeded at a density of 5,000 cells/well into a 96-well plate, and then administered saline (vehicle control), DEX (10 μM) or DEX (10 μM) plus irisin (1, 10 or 100 ng/ml), as previously described (22,37). The cells were cultured for 72 h at 37˚C and 5% CO_2 in an incubator. After adding 10 μl CCK-8 reagent to each well and incubating for 2 h, absorbance was recorded at 450 nm.

The cytotoxicity of DEX and irisin was tested using an LDH Cytotoxicity Detection kit (cat. no. MK401; Takara Bio, Inc.) according to the manufacturer's instructions. Briefly, cells were seeded at a density of $5x10^4$ cells/well in 12-well plates. Following 72 h administration of DEX (10 μM) and irisin (1, 10 or 100 ng/ml) at 37˚C, the LDH activity released into the culture supernatant was detected and normalized to total LDH activity (supernatant + cell lysate). The absorbance was read at 490 nm using a microplate reader (Multiskan FC; Thermo Fisher Scientific, Inc.). All experiments were performed with five replicates.

Annexin V assay. MC3T3-E1 cell apoptosis was assessed by flow cytometry using an Annexin V FITC apoptosis detection kit (cat. no. 556547; BD Biosciences) according to the manufacturer's instructions. Briefly, following 48 h DEX (10 μM) treatment in the presence or absence of irisin (100 ng/ml) at 37˚C, cells were resuspended in 500 μl binding buffer, incubated with 5 μl each Annexin V-FITC and propidium iodide (PI) for 15 min in the dark at room temperature, then analyzed using a BD FACSAria III flow cytometer (BD Biosciences). Data were analyzed using FlowJo version 10 (BD Biosciences). Total cell death was defined as the sum of PI- and Annexin V-positivity.

Co-immunoprecipitation (Co-IP) assay. MC3T3-E1 cells were treated with DEX (10 μM) with or without irisin (100 ng/ml) at 37˚C for 48 h, washed with ice-cold PBS, and lysed in ice-cold RIPA lysis buffer (Beyotime Biotechnology) containing protease and phosphatase inhibitors (Roche Diagnostics GmbH) for 30 min on ice. Lysates were centrifuged at 12,000 x g for 15 min at 4˚C, the supernatants were collected and protein concentrations were quantified using a BCA Protein Assay kit. An aliquot of the lysate was reserved as the input control. Equal amounts of protein (500 μg/reaction) were pre-cleared with 20 μl Protein A/G-agarose bead slurry per reaction (cat. no. sc-2003; Santa Cruz Biotechnology, Inc.) for 1 h at 4˚C with gentle rotation; the pre-cleared lysates were then divided equally and incubated overnight at 4˚C with

anti-ITGB5 (2 μg) or normal mouse IgG (2 μg) as a negative control. The immune complexes were captured with a further 20 μl of the same bead slurry for 4 h at 4˚C with gentle rotation, washed five times with ice-cold PBS and eluted by boiling in SDS-PAGE sample buffer for 10 min. The eluates and the input samples were separated by 10% SDS-PAGE, transferred onto PVDF membranes (MilliporeSigma) and subjected to western blotting for ITGB5 and irisin as aforementioned.

Reverse transcription-quantitative (RT-q)PCR. Total RNA was extracted from MC3T3-E1 cells using TRIzol® reagent (Invitrogen; Thermo Fisher Scientific, Inc.), and first-strand cDNA was synthesized using a RevertAid First Strand cDNA Synthesis kit (cat. no. K1622; Thermo Fisher Scientific, Inc.) according to the manufacturer's instructions (65˚C for 5 min, 42˚C for 60 min and 70˚C for 5 min). qPCR was performed using TransStart® Tip Green qPCR SuperMix (TransGen Biotech Co., Ltd.) with the following thermocycling conditions: Initial denaturation at 94˚C for 30 sec, followed by 40 cycles of 94˚C for 5 sec and 60˚C for 30 sec, followed by melt-curve analysis. Primer sequences are listed in Table SII. Relative gene expression was calculated using the $2^{-\Delta\Delta Cq}$ method (38) and normalized to Gapdh expression.

ROS assay and oxidative stress detection. MC3T3-E1 intracellular ROS levels were measured using dihydroethidium (DHE) staining, as previously described (39). Briefly, following 24 h treatment with DEX (10 μM) in the presence or absence of irisin (100 ng/ml) at 37˚C, the cells were fixed in 4% paraformaldehyde for 15 min at room temperature and stained with DHE (10 μM) for 30 min at 37˚C in the dark. Images of the cells were then captured under a fluorescence microscope (BX53; Olympus Corporation). Fluorescence intensity was calculated with ImageJ by two researchers blinded to the treatment groups.

Malondialdehyde (MDA; cat. no. S0131S), glutathione (GSH; cat. no. S0052) and total superoxide dismutase (SOD; cat. no. S0101S) levels in MC3T3-E1 cells were measured using commercial kits (Beyotime Biotechnology) according to the manufacturer's protocols. NADPH oxidase activity was measured using a commercial kit (cat. no. A127-1-1; Nanjing Jiancheng Bioengineering Institute) according to the manufacturer's instructions, as previously described (26).

Detection of apoptosis by ELISA. Cell apoptosis was quantified by a Cell Death Detection ELISAPLUS kit (cat. no. 11774425001; Roche Diagnostics GmbH) according to the manufacturer's instructions. This photometric sandwich immunoassay detects cytoplasmic histone-associated DNA fragments (mono- and oligonucleosomes). Briefly, cells were lysed and the cytoplasmic fraction was incubated with anti-histone-biotin and anti-DNA-peroxidase in streptavidin-coated wells for 2 h at room temperature; after washing, ABTS substrate was added and the absorbance was measured at 405 nm (reference, 490 nm) using a microplate reader (Multiskan FC; Thermo Fisher Scientific, Inc.). Values were normalized to the untreated control.

Lentivirus transduction. To knock down the expression of Nrf2, Bach1 and integrin (Itg)b5, short hairpin (sh)RNAs targeting Nrf2, Bach1 and Itgb5, together with a scrambled control shRNA (referred to hereafter as sh-C), were cloned into the lentiviral vector LV3 (H1/GFP&Puro) (Shanghai GenePharma Co., Ltd.). Lentiviral particles were generated by co-transfecting 293T cells (cat. no. CRL-3216; American Type Culture Collection) with the transfer (10 μg), packaging (psPAX2; 7.5 μg) and envelope (pMD2.G; 5 μg) plasmids at a ratio of 4:3:2 using Lipofectamine® 3000 (Invitrogen; Thermo Fisher Scientific, Inc.) at 37˚C for 6 h. Subsequently, the supernatants were harvested at 48 and 72 h, centrifuged and filtered (0.45 μm). MC3T3-E1 cells were seeded in 6-well plates at a density of $1x10^5$ cells/well and, at ~50% confluence, were transduced with the viral supernatant at a multiplicity of infection of 50 in the presence of polybrene (5 μg/ml) for 24 h at 37˚C. Stable clones were then selected with puromycin (2 μg/ml) for 10 days and maintained in 1 μg/ml puromycin. The targeting sequences of the shRNA constructs were as follows: sh-C, 5'-CAACAAGATGAAGAGCACCAA-3'; Nrf2 sh1, 5'-CCAAAGCTAGTATAGCAATAA-3'; Nrf2 sh2, 5'-GCCTTACTCTCCCAGTGAATA-3'; Bach1 shRNA, 5'-GCGTACACAATATCGAGGAAT-3'; and Itgb5 shRNA, 5'-CGCCTTCAACAAGTTCAACAA-3'. Knockdown efficiency was confirmed by RT-qPCR for all targets and by western blotting for Nrf2, demonstrating ~95% reduction in Nrf2 expression, 70% reduction in Bach1 and 95% reduction in Itgb5 in the stable cell lines. Stable cell lines were used for all subsequent experiments.

Detection of mitochondrial membrane potential (MMP). MMP was measured using JC-1 MMP Assay Kit (cat. no. C2006; Beyotime Biotechnology) according to the manufacturer's protocols. Briefly, MC3T3-E1 cells were seeded in 12-well tissue culture plates at $5x10^4$ cells/well. Following 24 h treatment with DEX (10 μM) in the presence or absence of irisin (100 ng/ml) at 37˚C, the cells were stained with JC-1 working solution (2 μM) for 20 min at 37˚C in the dark, washed twice with JC-1 staining buffer, and images were captured under a fluorescence microscope (BX53; Olympus Corporation). The JC-1 aggregate/monomer (red/green) fluorescence ratio was quantified using ImageJ.

Leptomycin B (LMB) treatment. To inhibit chromosome region maintenance 1 (CRM1)-dependent nuclear export, cells were pretreated with LMB (cat. no. L2913; Sigma-Aldrich; Merck KGaA) at 20 nM in serum-containing medium for 1 h at 37˚C, after which the cells were incubated with DEX (10 μM) with or without irisin (100 ng/ml) for the indicated times (24 h for immunofluorescence, DHE and JC-1 staining; 48 h for western blotting) in the continued presence of LMB. Control cells received an equal volume of vehicle (methanol:water, 7:3).

Cilengitide treatment. To inhibit ITG αVβ5, cells were pretreated with 10 μM cilengitide (cat. no. HY-16141; MedChemExpress) in serum-containing medium for 1 h at 37˚C, after which the cells were incubated with DEX (10 μM) with or without irisin (100 ng/ml) for 24 h (immunofluorescence) or 48 h (western blotting) in the continued presence of cilengitide. Control cells received an equal volume of vehicle (DMSO; final concentration ≤0.1%).

Immunofluorescence assay. Immunofluorescence staining was performed as previously described (40). Briefly, MC3T3-E1 cells grown on coverslips were treated with DEX (10 μM) with or without irisin (100 ng/ml) for 24 h at 37˚C, in the presence or absence of cilengitide or LMB as indicated. The cells were then fixed in 4% paraformaldehyde for 15 min at room temperature, permeabilized with 0.1% Triton X-100 for 10 min and blocked with 10% normal goat serum for 30 min at 37˚C. For the co-localization of irisin and ITG αVβ5, the cells were incubated overnight at 4˚C with rabbit anti-irisin and mouse anti-ITG αV/β5 antibodies, followed by incubation with Alexa Fluor® 488-conjugated goat anti-rabbit IgG and Alexa Fluor 594-conjugated goat anti-mouse IgG for 1 h at room temperature in the dark. For the detection of Bach1 and F-actin, the cells were incubated overnight at 4˚C with rabbit anti-Bach1 antibody, followed by incubation with Alexa Fluor 488-conjugated goat anti-rabbit IgG for 1 h at room temperature in the dark; F-actin was stained with Alexa Fluor 594-conjugated phalloidin for 30 min at room temperature in the dark. In both cases, nuclei were counterstained with DAPI and the cells were mounted with an anti-fade mounting medium. Images were acquired using a confocal microscope (TCS SP8 STED 3X; Leica Microsystems GmbH) with LAS X software (Leica Microsystems GmbH); co-localization and nuclear Bach1 fluorescence intensity were analyzed using ImageJ.

Subcellular fractionation. Nuclear and cytoplasmic protein fractions were prepared using the NE-PER™ Nuclear and Cytoplasmic Extraction Reagents (cat. no. 78833; Thermo Fisher Scientific, Inc.) according to the manufacturer's instructions. Briefly, MC3T3-E1 cells were washed twice with ice-cold PBS and lysed in ice-cold CER I buffer supplemented with protease and phosphatase inhibitors. Following the addition of CER II buffer and centrifugation at 16,000 x g for 5 min at 4˚C, the supernatant was collected as the cytoplasmic fraction. The pellet was resuspended in ice-cold NER buffer, vortexed for 15 sec every 10 min over 40 min at 4˚C, and centrifuged at 16,000 x g for 10 min at 4˚C; the resulting supernatant was collected as the nuclear fraction. Protein concentrations were determined using a BCA Protein Assay kit, and equal amounts of nuclear protein were separated by 10% SDS-PAGE and subjected to western blotting as aforementioned. Nrf2 and Bach1 levels in the nuclear fractions were normalized to PCNA, which served as the nuclear loading control.

U0126 treatment. To inhibit MEK/Erk signaling, cells were pretreated with 10 μM U0126 (cat. no. 9903; Cell Signaling Technology, Inc.) in serum-containing medium for 1 h at 37˚C, after which the cells were incubated with DEX (10 μM) with or without irisin (100 ng/ml) for 48 h in the continued presence of U0126. Control cells received an equal volume of vehicle (DMSO; final concentration ≤0.1%).

Statistical analysis. All tests were conducted ≥3 times, and the results are presented as the mean ± SD. Multiple groups were compared using one-way ANOVA followed by Tukey's post hoc test for pairwise comparisons. Comparisons between two groups were performed using independent-sample t-tests. $P<0.05$ was considered to indicate a statistically significant difference. All statistical analyses were performed using SPSS 20.0 (IBM Corp.).

Results

Irisin inhibits MPS-induced ONFH in rats. To evaluate the effect of irisin on GC-induced ONFH, a rat model was established by intramuscular injection of MPS (Fig. 1A). The incidence rates of ONFH were 0.0 (0/18) in the Control group, 80.0 (12/15) in the Model and 12.5% (2/16) in the Irisin group. Histomorphometric analysis of H&E-stained FH sections (Fig. 1B) revealed marked ON in the Model group, characterized by sparse and disorganized Tb bone, as well as abundant empty osteocyte lacunae within the subchondral region. By contrast, irisin-treated animals exhibited well-preserved Tb architecture and a notable decrease in the number of empty lacunae. To evaluate the subchondral Tb architecture of FHs, micro-CT was used. The Model group exhibited notable structural changes in subchondral trabeculae, including bone mass loss and cystic degeneration, compared with the Control (Fig. 1C). In the Irisin group subchondral trabeculae were relatively intact and well distributed. Quantitative analysis of microstructural parameters (Fig. 1D-G) confirmed that MPS significantly decreased BV, BV/TV and Tb.Th, while increasing Tb.Sp. Conversely, irisin significantly reversed these deleterious changes, restoring BV, BV/TV and Tb.Th, and decreasing Tb.Sp relative to the Model group. Collectively, these results indicated that irisin effectively attenuated MPS-induced ON and Tb bone loss in the FH.

The present study examined the protective mechanisms of irisin by assessing oxidative stress and apoptosis in the FH. Compared with the Control group, the Model group exhibited significantly elevated levels of ROS, as detected by DHE fluorescence staining, however, irisin treatment significantly decreased ROS accumulation (Fig. 2A and C). Consistently, IHC analyses revealed that irisin upregulated the expression of the antioxidant enzymes HO-1 and NQO1 in FH sections (Fig. 2B, D and E). TUNEL staining demonstrated that irisin significantly attenuated MPS-induced apoptosis in osteocytes and osteoblasts in the FH (Fig. 2F and H). Concurrently, IHC analysis of total and cleaved caspase-3 in FH sections showed that MPS increased the immunoreactivity of both forms, whereas irisin markedly reduced cleaved caspase-3 without substantially altering total caspase-3 expression (Fig. 2G, I and J). Western blot analysis of FH tissue confirmed these observations at the molecular level, showing that irisin upregulated the anti-apoptotic protein BCL-2 and downregulated the pro-apoptotic proteins BAX and cleaved caspase-3, thereby restoring the BAX/BCL-2 ratio toward control levels and inhibiting the caspase-3 activation pathway (Fig. 2K-P). Collectively, these results suggested that irisin may protect against MPS-induced ONFH by simultaneously suppressing oxidative stress and apoptosis in the FH.

Irisin suppresses DEX-induced oxidative stress in vitro in a Nrf2-dependent manner. It has been shown in previous studies that DEX induces intracellular ROS production, leading to oxidative stress injury and cell death in osteoblasts (41,42). To determine the role of Nrf2, shRNA-mediated knockdown was performed, Nrf2 mRNA levels were markedly reduced in

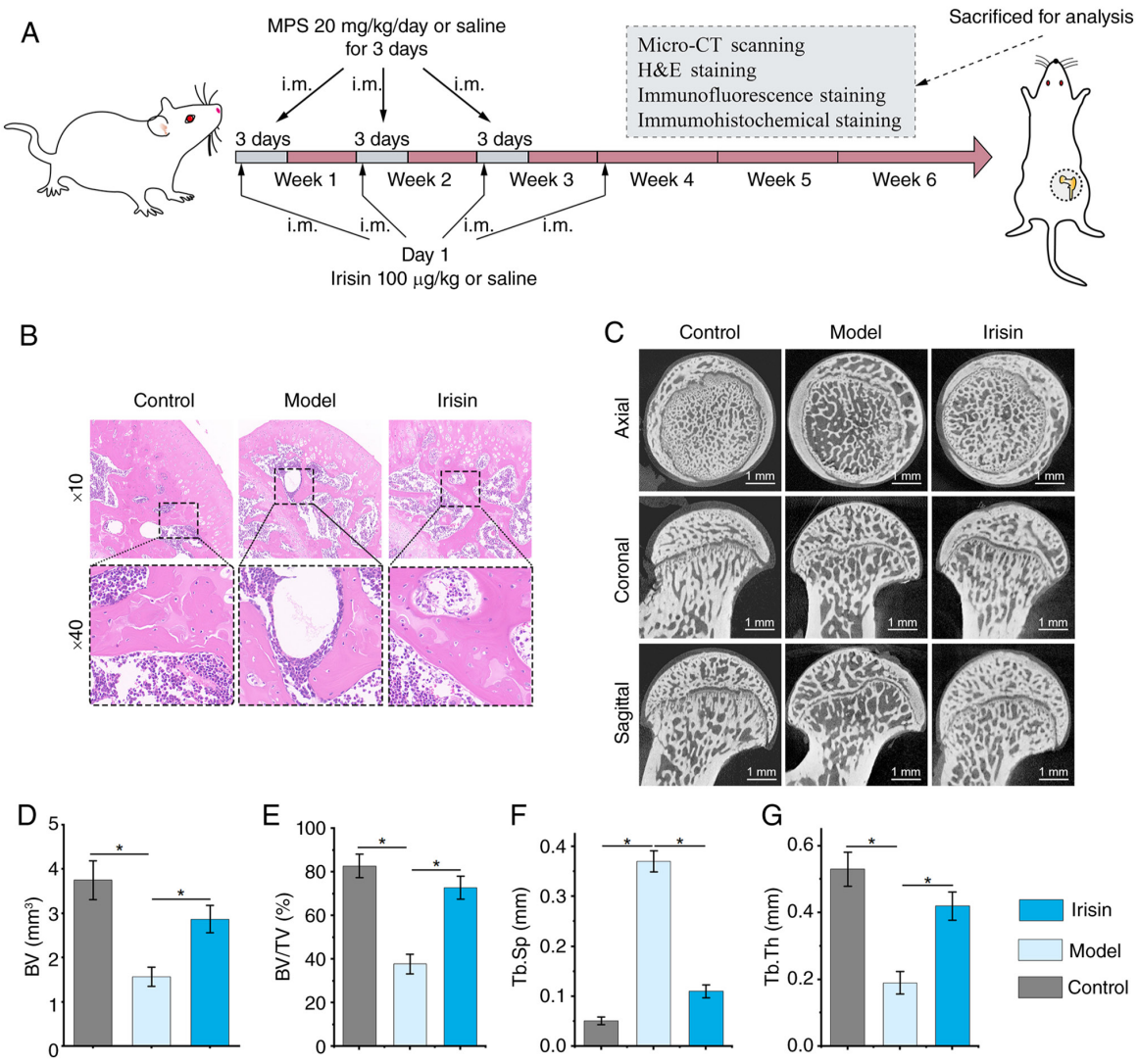


Figure 1. Irisin attenuates MPS-induced ONFH in rats. (A) Schematic diagram of the establishment of MPS-induced rat ONFH model and irisin administration. (B) Representative H&E staining of FH. (C) Micro-CT analysis of FH morphology. Representative 3D reconstructions from axial, coronal and sagittal views are presented. Quantitative analysis of (D) BV, (E) BV/TV, (F) Tb.Sp and (G) Tb.Th. Data are presented as the mean ± SD. *P<0.05. BV, bone volume; CT, computed tomography; H&E, hematoxylin and eosin; i.m., intramuscular; MPS, methylprednisolone; ONFH, osteonecrosis of the femoral head; Sp, separation; Tb, trabecular; Th, thickness; TV, total volume.

sh-Nrf2 cells compared with in sh-C cells (Fig. 3A). To investigate the cellular mechanisms underlying irisin-mediated protection against oxidative stress, MC3T3-E1 osteoblasts were exposed to DEX with or without irisin. DEX significantly increased intracellular ROS levels, as evidenced by intensified DHE fluorescence, which was effectively attenuated by irisin co-treatment (Fig. 3B and C). Notably, Nrf2 silencing largely abolished the antioxidant effect of irisin, with ROS levels comparable to those in the DEX group (Fig. 3B and C). Furthermore, DEX induced notable MMP dissipation, indicated by the loss of JC-1 aggregates (red fluorescence) and increased green monomer fluorescence, whereas irisin preserved MMP; this protection was abrogated by Nrf2 knockdown (Fig. 3D and E). Biochemically, DEX resulted in elevated MDA levels and NADPH oxidase activity, alongside depletion of GSH and SOD; irisin co-administration reversed these alterations (Fig. 3F-I). At the molecular level, western blot analysis revealed that DEX significantly increased the expression of p67phox, and decreased the expression levels of SOD1 and SOD2; irisin co-treatment reversed these DEX-induced alterations, restoring SOD1 and SOD2 expression, and reducing p67phox expression. These effects were blocked by Nrf2 silencing (Fig. 3J-M). Collectively, these findings indicated that irisin may mitigate DEX-induced oxidative stress in a Nrf2-dependent manner, thereby preserving mitochondrial integrity and enhancing cellular antioxidant defenses.

Irisin alleviates DEX-induced osteoblast apoptosis in vitro in a Nrf2-dependent manner. To evaluate the cytoprotective effect of irisin on GC-injured osteoblasts, cell viability and membrane integrity were assessed. Irisin dose-dependently restored the cell viability compromised by DEX, as determined by CCK-8 assay (Fig. 4A) and significantly decreased DEX-induced LDH release (Fig. 4B). These results indicated that irisin can improve cell survival under GC stress.

The present study also examined apoptosis. ELISA quantification of cytoplasmic histone-associated DNA fragments

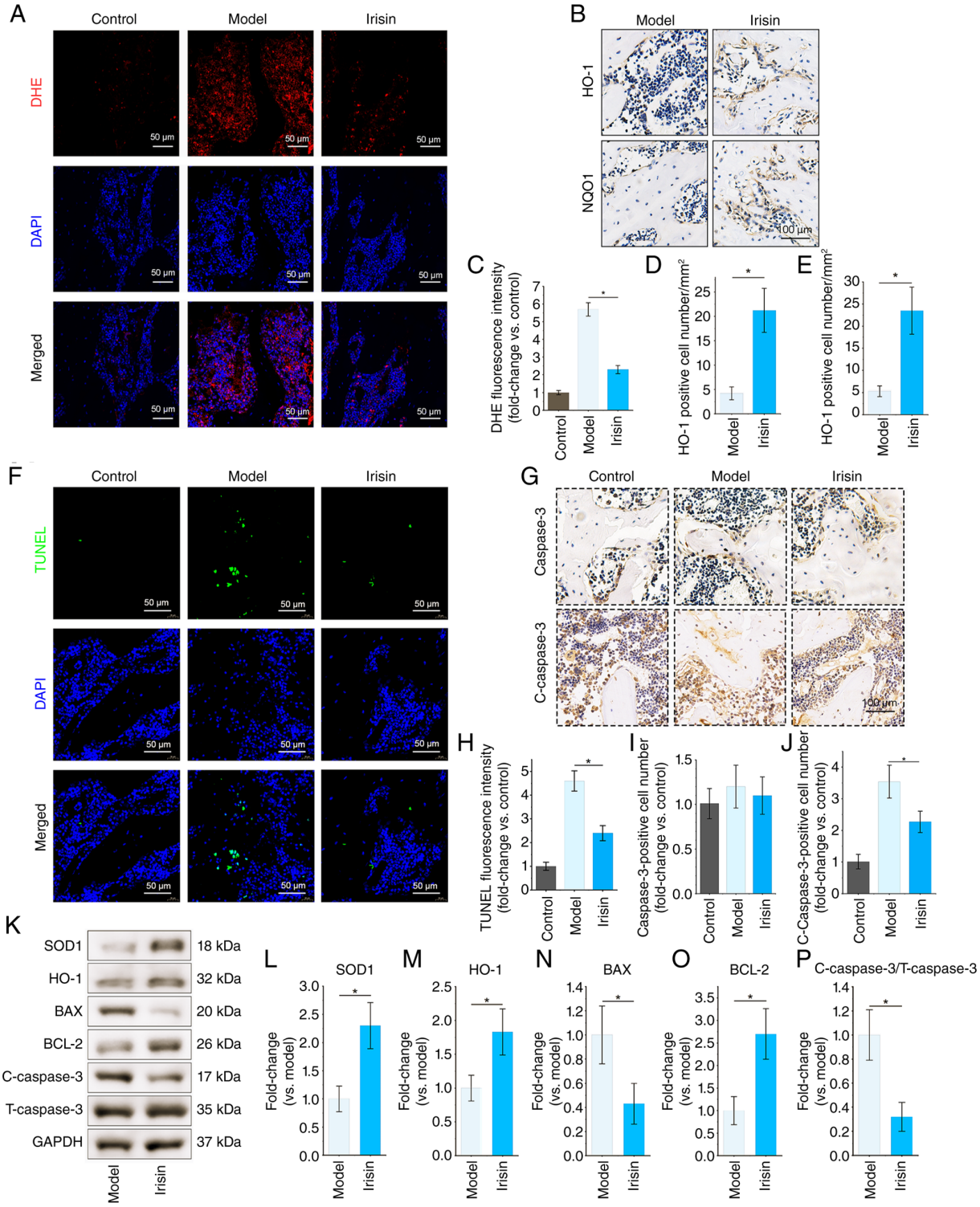


Figure 2. Irisin suppresses oxidative stress and attenuates apoptosis in methylprednisolone-induced osteonecrosis of the femoral head. (A) Representative images of DHE staining for the detection of reactive oxygen species. (B) Immunohistochemical staining for antioxidant enzymes HO-1 and NQO1 (brown, positive signal; blue, hematoxylin-counterstained nuclei). (C) Quantitative analysis of the DHE fluorescence intensity. Numbers of (D) HO-1-positive cells and (E) NQO1-positive cells. (F) Representative images of TUNEL staining for the detection of apoptotic cells. (G) Immunohistochemical staining for caspase-3 and C-caspase-3; brown staining indicates positive immunoreactivity and nuclei were counterstained with hematoxylin (blue). (H) Quantification of TUNEL-positive cells. Numbers of (I) T-caspase-3-positive cells and (J) C-caspase-3-positive cells. (K) Western blot analysis of oxidative stress- and apoptosis-associated proteins in femoral head tissue. Semi-quantitative analysis of (L) SOD1, (M) HO-1, (N) BAX, (O) BCL-2 and (P) ratio of C- to T-caspase-3. Data are presented as the mean ± SD. *P<0.05. C, cleaved; HO, heme oxygenase; NQO, NAD(P)H quinone oxidoreductase; T, total.

(mono- and oligonucleosomes) showed that irisin co-treatment markedly attenuated DEX-induced apoptosis in a dose-dependent manner (Fig. 4C). Furthermore, TUNEL staining confirmed that irisin reduced the proportion of apoptotic cells, with greater protection observed at the high compared with the low dose (Fig. 4D and E).

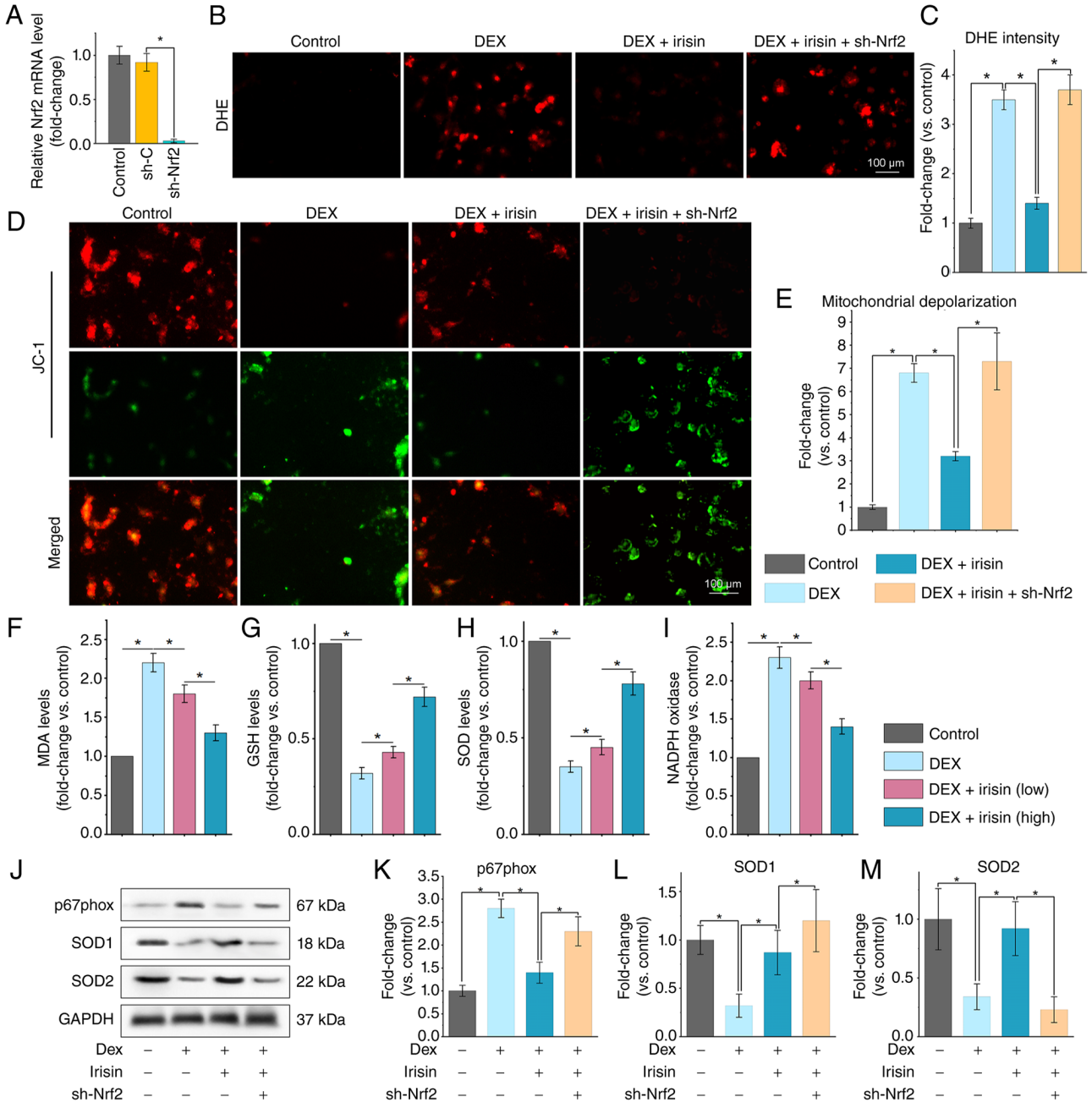


Figure 3. Irisin suppresses DEX-induced oxidative stress *in vitro* in a Nrf2-dependent manner. (A) Validation of Nrf2 knockdown. Relative Nrf2 mRNA levels in Control, sh-C and sh-Nrf2 cells, as determined by reverse transcription-quantitative PCR. (B) Representative DHE fluorescence imaging of intracellular reactive oxygen species levels. (C) Quantification of DHE fluorescence intensity. (D) Representative JC-1 staining indicating mitochondrial membrane potential (red, aggregates; green, monomers). (E) Quantification of JC-1 aggregate/monomer ratio. Biochemical analyses of (F) MDA, (G) GSH, (H) SOD and (I) NADPH oxidase levels. (J) Western blot analysis of oxidative stress-associated proteins. Semi-quantification of (K) p67phox, (L) SOD1 and (M) SOD2. Data are presented as the mean ± SD. *P<0.05. DEX, dexamethasone; DHE, dihydroethidium; GSH, glutathione; MDA, malondialdehyde; sh, short hairpin; sh-C, control shRNA; SOD, superoxide dismutase.

To substantiate the anti-apoptotic effect of irisin, flow cytometry with Annexin V/PI double staining and western blot analysis were performed. DEX significantly increased the population of apoptotic cells, which was significantly suppressed by irisin co-treatment. Notably, this protective effect was largely reversed following Nrf2 silencing by shRNA (Fig. 4F-J). Consistently, western blot analysis revealed that DEX markedly increased BAX expression and decreased BCL-2 expression, thereby elevating the BAX/BCL-2 ratio, and increased the cleaved caspase-3/total caspase-3 ratio; irisin co-treatment reversed these alterations, restoring BCL-2 expression, and reducing BAX and cleaved caspase-3 toward control levels. These regulatory effects were also inhibited by Nrf2 knockdown (Fig. 4K-N). Collectively, these findings demonstrated that irisin protects osteoblasts from DEX-induced apoptosis in a Nrf2-dependent manner.

Irisin activates the Nrf2 signaling pathway to counteract oxidative stress. As Nrf2 is a master regulator of the cellular antioxidant response and its activation has been implicated in

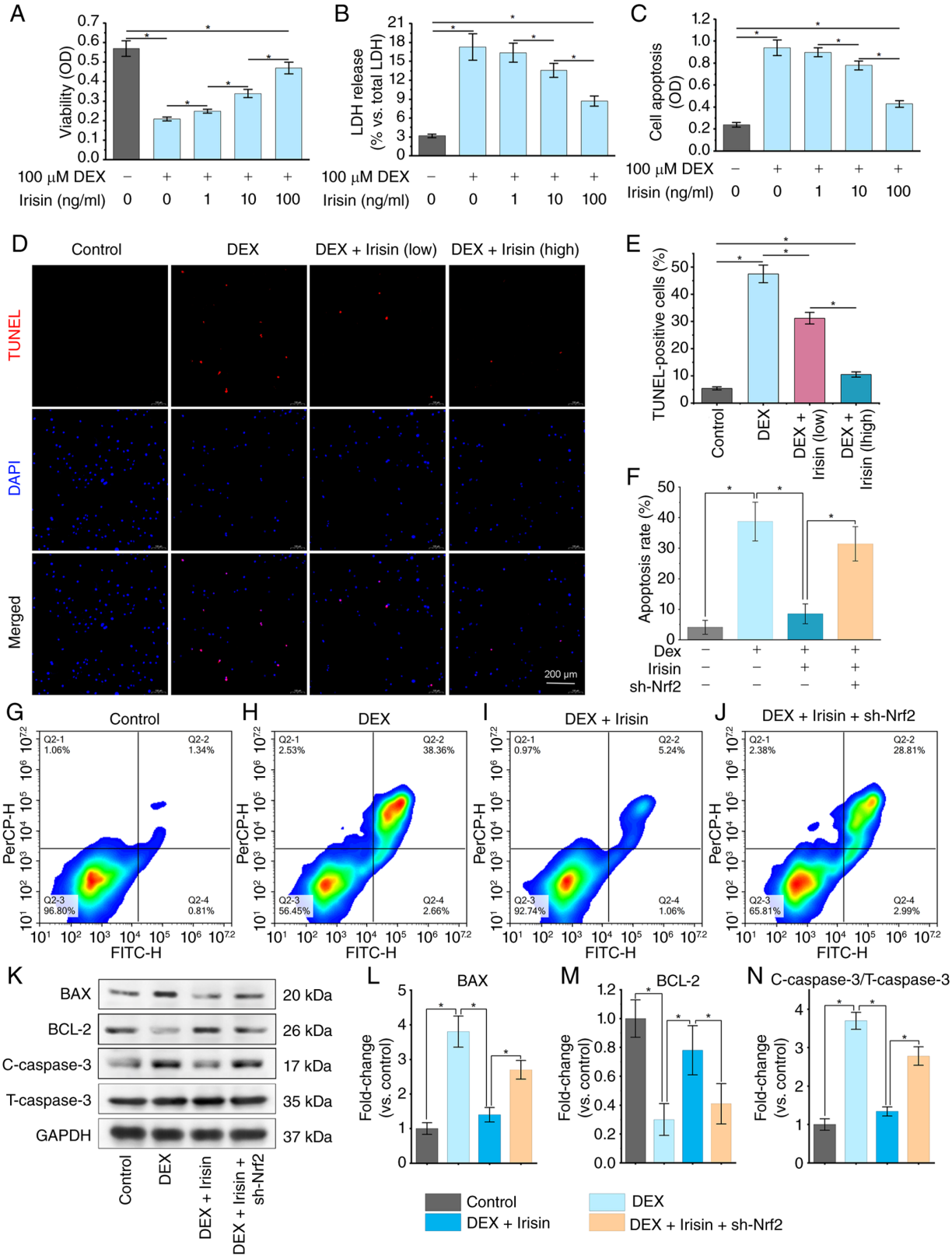


Figure 4. Irisin alleviates DEX-induced osteoblast apoptosis in a Nrf2-dependent manner. (A) Cell Counting Kit 8 assay for cell viability. (B) LDH release assay. (C) ELISA detection of early apoptosis. (D) Representative TUNEL staining images. (E) Quantification of TUNEL-positive cells. (F) Quantification of apoptotic cells. Representative flow cytometry plots of Annexin V/PI double staining in the (G) Control, (H) DEX, (I) DEX + irisin and (J) DEX + irisin + sh-Nrf2 groups. (K) Western blot analysis of BAX, BCL-2 and C-caspase-3. Semi-quantification of (L) BAX, (M) BCL-2 and (N) the ratio of C- to T-caspase-3. Data are presented as the mean ± SD. *P<0.05. C, cleaved; DEX, dexamethasone; LDH, lactate dehydrogenase; OD, optical density; sh, short hairpin; T, total.

cytoprotection (6,8,43), the present study aimed to elucidate the molecular mechanism underlying the protective effect of irisin. It was hypothesized that irisin mitigates oxidative stress by modulating the Nrf2 pathway. DEX significantly

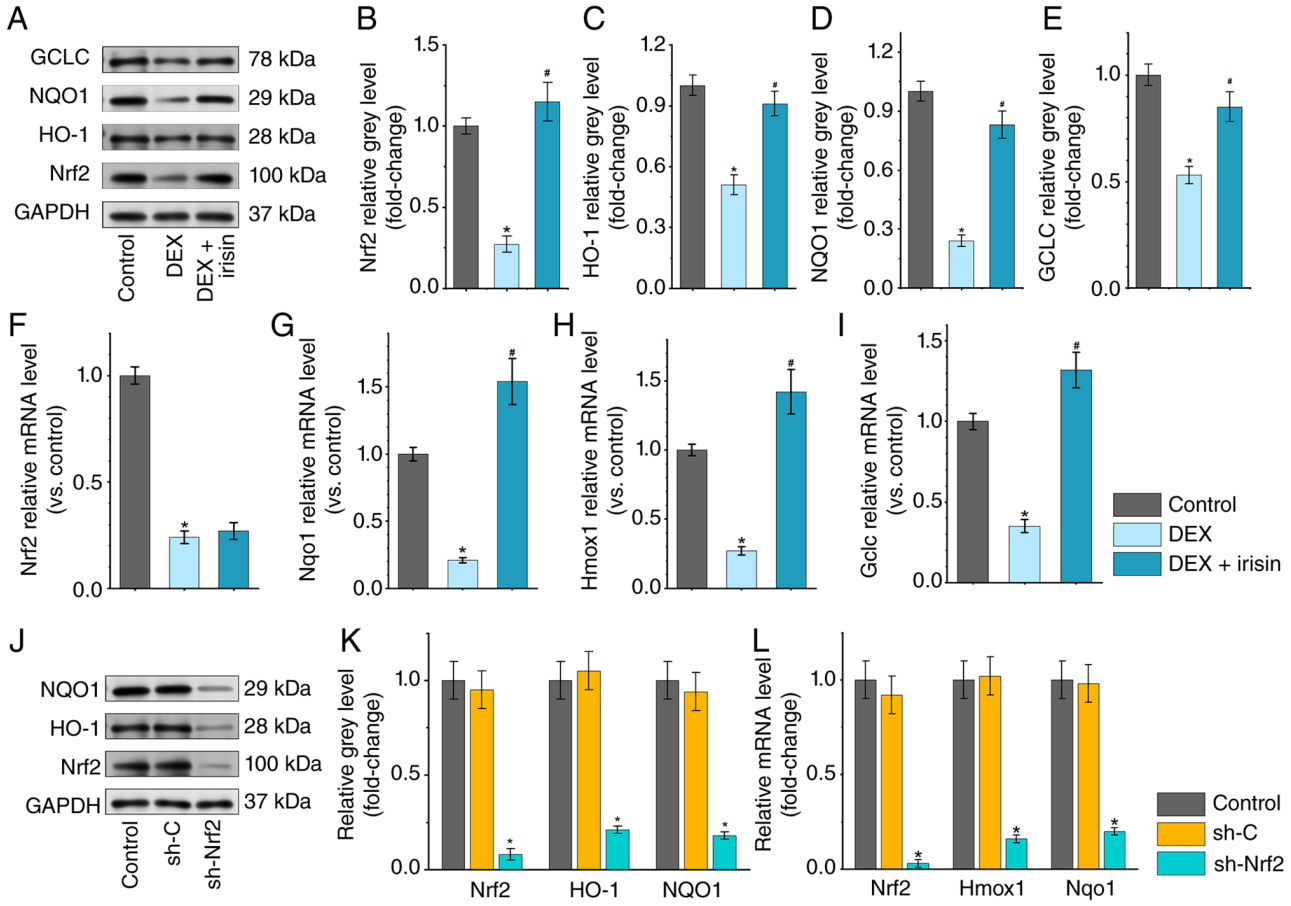


Figure 5. Irisin activates the Nrf2 signaling pathway to counteract oxidative stress. (A) Western blot analysis and semi-quantification of (B) Nrf2, (C) HO-1, (D) NQO1 and (E) GCLC protein expression. Relative mRNA levels of (F) Nrf2, (G) Nqo1, (H) Hmox1 and (I) Gclc. (J) Western blot analysis and semi-quantification of (K) Nrf2, HO-1 and NQO1 in cells transfected with sh-Nrf2 or sh-C. (L) Quantification of Nrf2, Hmox1 and Nqo1 mRNA levels. Data are presented as the mean ± SD. *P<0.05 vs. Control; #P<0.05 vs. DEX. DEX, dexamethasone; GCLC, glutamate-cysteine ligase catalytic subunit; HO-1/Hmox1, heme oxygenase-1; NQO1, NAD(P)H quinone oxidoreductase 1; sh, short hairpin; sh-C, control shRNA.

decreased the protein expression of Nrf2 in MC3T3-E1 cells (Fig. 5A and B), whereas co-treatment with irisin reversed this DEX-induced downregulation, restoring Nrf2 protein levels. As Nrf2 functions primarily as a transcription factor (10,11), the present study examined its downstream targets. Consistent with the DEX-induced decrease and the irisin-induced restoration of Nrf2 protein, DEX significantly reduced the protein levels of HO-1, NQO1 and GCLC, whereas co-treatment with irisin significantly upregulated all three relative to the DEX group, restoring them toward control levels (Fig. 5A and C-E). To determine whether this upregulation occurred at the transcriptional level, the present study quantified the mRNA expression levels of these genes. Irisin markedly elevated the mRNA levels of Hmox1, Nqo1 and Gclc in the presence of DEX (Fig. 5F-I). Notably, irisin co-treatment did not significantly restore the DEX-induced reduction in Nrf2 mRNA levels (Fig. 5F), which remained significantly lower than in the control group, whereas Nrf2 protein expression was fully restored by irisin (Fig. 5B). This dissociation between Nrf2 mRNA and protein levels suggests that irisin acts post-translationally, most likely by stabilizing the Nrf2 protein. To confirm the role of Nrf2 in mediating irisin-induced antioxidant effects, shRNA-mediated knockdown was performed (Fig. 5J-L). Knockdown of Nrf2 markedly decreased Nrf2 protein and mRNA levels and, consequently, reduced the expression of both NQO1 and HO-1 at the protein and mRNA levels (Fig. 5J-L), confirming that the expression of these antioxidant enzymes requires Nrf2. Collectively, these findings demonstrated that irisin may alleviate DEX-induced oxidative injury by activating the Nrf2 signaling pathway, primarily via a post-translational mechanism that stabilizes the Nrf2 protein and enhances the transcription of antioxidant genes.

Irisin promotes Bach1 nuclear export to facilitate Nrf2 nuclear accumulation and exert cytoprotection. To elucidate how irisin activates Nrf2, the present study examined the expression of Keap1, the canonical cytoplasmic suppressor of Nrf2. Western blot analysis showed that irisin did not significantly alter Keap1 protein levels compared with DEX treatment alone (Fig. 6A and B). Subcellular distribution of Nrf2 and its competitive suppressor Bach1 was subsequently assessed. Subcellular fractionation revealed that irisin significantly increased Nrf2 nuclear accumulation while decreasing nuclear Bach1 levels (Fig. 6C-E). Immunofluorescence staining confirmed that irisin decreased Bach1 nuclear retention (Fig. 6F and H). Therefore, it was hypothesized that the promoting effect of irisin on Nrf2 may be associated with its facilitation of Bach1 nuclear export.

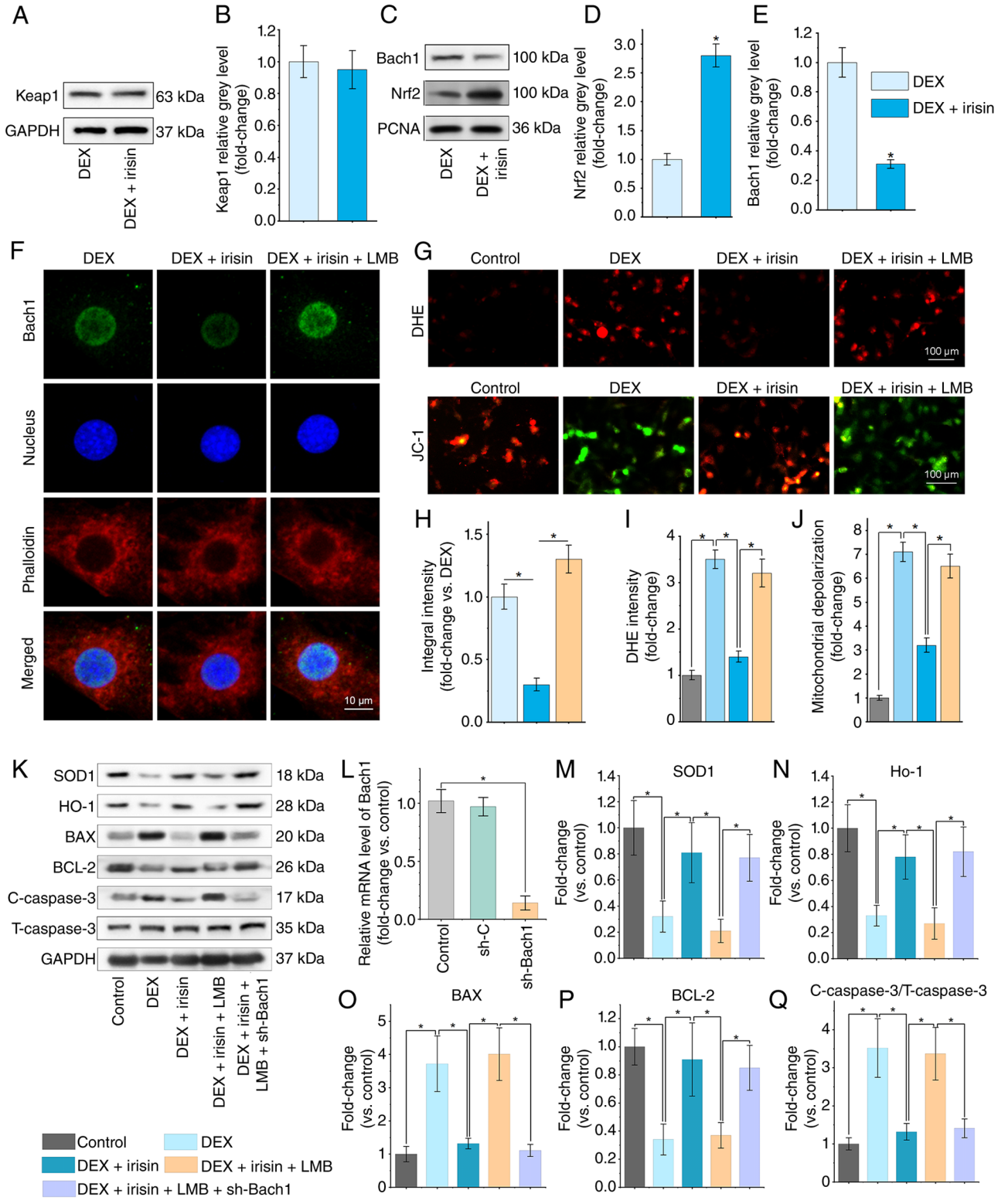


Figure 6. Irisin promotes Bach1 nuclear export to facilitate Nrf2 activation and cytoprotection. (A) Western blot analysis and semi-quantification of (B) Keap1 protein expression. (C) Western blot analysis and semi-quantification of (D) Nrf2 and (E) Bach1 in nuclear fractions. (F) Immunofluorescence staining of Bach1 (green) and DAPI (blue). (G) DHE staining for ROS and JC-1 staining for MMP. Quantification of (H) nuclear Bach1 fluorescence intensity, (I) ROS levels and (J) MMP (red/green ratio). (K) Western blot analysis. (L) Relative mRNA expression levels of Bach1 in Control, sh-C and sh-Bach1 cells. Semi-quantification of (M) SOD1, (N) HO-1, (O) BAX, (P) BCL-2 and (Q) C-caspase-3. Data are presented as the mean ± SD. *P<0.05 vs. DEX or as indicated. C, cleaved; DEX, dexamethasone; DHE, dihydroethidium; HO-1, heme oxygenase-1; Keap1, Kelch-like ECH-associated protein 1; LMB, leptomycin B; MMP, mitochondrial membrane potential; PCNA, proliferating cell nuclear antigen; ROS, reactive oxygen species; SOD, superoxide dismutase; T, total; sh, short hairpin; sh-C, control shRNA.

To verify whether Bach1 nuclear export is required for irisin-induced protective effects, cells were treated with LMB, a CRM1-dependent nuclear export inhibitor. LMB significantly blocked the irisin-induced decrease in nuclear Bach1

(Fig. 6F and H). Functionally, LMB abolished the ability of irisin to attenuate intracellular ROS generation (Fig. 6G and I), restore MMP (Fig. 6G and J), upregulate HO-1 and SOD1 (Fig. 6K, M and N) and modulate apoptotic proteins (BCL-2 upregulation; BAX and cleaved caspase-3 downregulation; Fig. 6K and P-Q). These data indicated that irisin-induced cytoprotective effects depend on Bach1 nuclear export.

To establish the causal role of Bach1, shRNA-mediated knockdown of Bach1 was performed; Bach1 mRNA levels were markedly reduced in sh-Bach1 compared with sh-C cells (Fig. 6L). Functionally, LMB abolished the ability of irisin to attenuate intracellular ROS generation and to restore MMP (Fig. 6G, I and J). In Bach1-knockdown cells, LMB failed to block the protective effects of irisin, as shown by the restored expression of SOD1, HO-1 and BCL-2, and the reduced expression of BAX and cleaved caspase-3 relative to cells treated with DEX + irisin + LMB (Fig. 6K and M-Q). These results demonstrated that the inhibitory effect of LMB on irisin may be dependent on the presence of Bach1. Collectively, these findings indicated that irisin can promote CRM1-dependent nuclear export of Bach1, thereby relieving Bach1-mediated suppression of Nrf2 and enabling Nrf2 nuclear accumulation to drive antioxidant and anti-apoptotic gene expression.

Irisin activates Erk1 signaling via ITG αVβ5 to promote Bach1 nuclear export. Having established that irisin promotes CRM1-dependent nuclear export of Bach1, the present study investigated the upstream signaling events governing this process. As Erk1/2 phosphorylation is implicated in Bach1 nuclear translocation (44), the present study examined the effect of irisin on Erk1 activation. Western blot analysis revealed that irisin significantly increased the phosphorylation of Erk1 in DEX-treated MC3T3-E1 cells, without altering total Erk1 levels (Fig. 7A and B). To determine whether Erk1 activation is required for irisin-induced Bach1 nuclear export, cells were pretreated with U0126, a specific MEK/Erk inhibitor. U0126 prevented the irisin-mediated reduction of nuclear Bach1 (Fig. 7C and D) and blocked the irisin-induced upregulation of Nrf2 target genes, Hmox1, Nqo1 and Gclc (Fig. 7E-G). These results are consistent with a requirement for MEK/Erk signaling in irisin-mediated Bach1 nuclear export and subsequent Nrf2 activation.

Previous studies have identified ITG αVβ5 as a functional receptor for irisin in various cell types, including intestinal epithelial cells, osteocytes and adipocytes (40,45,46). To verify this interaction in the present experimental system, immunofluorescence double staining was performed. Confocal microscopy revealed prominent colocalization of irisin with ITG αVβ5 on the surface of DEX + irisin-treated osteoblasts (Fig. 7H). To provide biochemical evidence for a physical interaction, the present study performed co-IP assay. Immunoprecipitation with an anti-ITGB5 antibody followed by immunoblotting for irisin detected a specific band at 24 kDa, whereas only a faint non-specific signal was observed in the IgG control (Fig. 7I). These data demonstrated that irisin may physically associate with ITG αVβ5 in osteoblasts. To assess the functional relevance of this interaction, the present study employed both pharmacological and genetic approaches. Treatment with cilengitide, an ITG αV inhibitor, significantly attenuated irisin-induced Erk1 phosphorylation (Fig. 7K and L) and prevented the irisin-mediated reduction of nuclear Bach1 (Fig. 7M and N). To achieve greater specificity, ITGB5 was silenced using shRNA (sh-Itgb5) (Fig. 7J). Knockdown of Itgb5 phenocopied the effects of cilengitide: Irisin failed to induce Erk1 phosphorylation (Fig. 7K and L) and decrease nuclear Bach1 levels (Fig. 7M and N). Collectively, these results established that irisin may engage ITG αVβ5 to activate Erk1 signaling, which in turn drives CRM1-dependent Bach1 nuclear export, enabling Nrf2 nuclear accumulation and antioxidant gene expression.

Discussion

GC-induced ONFH is a debilitating orthopedic condition characterized by progressive bone cell death and articular collapse (3,43). Although the pathogenesis of ONFH is multifactorial, mounting evidence indicates that excessive oxidative stress and osteoblast apoptosis serve pivotal roles in its development (4-6,40). In the present study, irisin, a myokine derived from FNDC5, effectively protected against GC-induced ONFH both *in vivo* and *in vitro*, with the underlying molecular mechanism involving the ITG αVβ5/Erk1/Bach1/Nrf2 signaling pathway.

The present *in vivo* results showed that irisin administration significantly decreased the incidence of MPS-induced ONFH in rats, preserved Tb bone microarchitecture and attenuated oxidative stress and apoptosis in FH tissue, as evidenced by DHE staining, TUNEL assay and IHC analysis of HO-1 and NQO1. These findings are consistent with previous reports on the role of irisin in bone metabolism (25,34,44,45). Colaianni *et al* (25) reported that low-dose irisin administration increased cortical bone mass and modulated osteoblast gene expression *in vivo* without inducing adipose tissue browning. Zhang *et al* (34) demonstrated that exercise-induced irisin promoted bone formation and systemic irisin administration revealed new regulatory mechanisms in bone metabolism. Zhu *et al* (44) generated osteoblast-lineage-specific FNDC5/irisin knockout mice and demonstrated that irisin deficiency led to lower bone density, delayed bone development and impaired exercise-induced bone strengthening. *In vitro*, irisin protected MC3T3-E1 osteoblasts from DEX-induced oxidative stress and apoptosis in a dose-dependent manner. Mechanistically, irisin activated the Nrf2 signaling pathway, as evidenced by increased nuclear accumulation of Nrf2 and upregulation of its downstream target genes, including Hmox1, Nqo1 and Gclc. This is in line with the study by Zhang *et al* (26), which demonstrated that FNDC5/irisin alleviated oxidative stress and cardiomyocyte apoptosis via Nrf2 activation in a doxorubicin-induced cardiotoxicity model. Notably, shRNA-mediated knockdown of Nrf2 abolished irisin-induced protective effects against ROS accumulation, MMP loss and apoptosis, confirming that Nrf2 is essential for irisin-mediated cytoprotection.

The present study identified Bach1 as a key mediator linking irisin to Nrf2 activation. Under physiological conditions, Bach1 competes with Nrf2 for binding AREs, thereby suppressing the transcription of antioxidant genes (12). Wang *et al* (13) recently demonstrated that the Bach1/HO-1 pathway may serve a crucial role in regulating oxidative stress and ferroptosis, highlighting the importance of this regulatory axis in cell

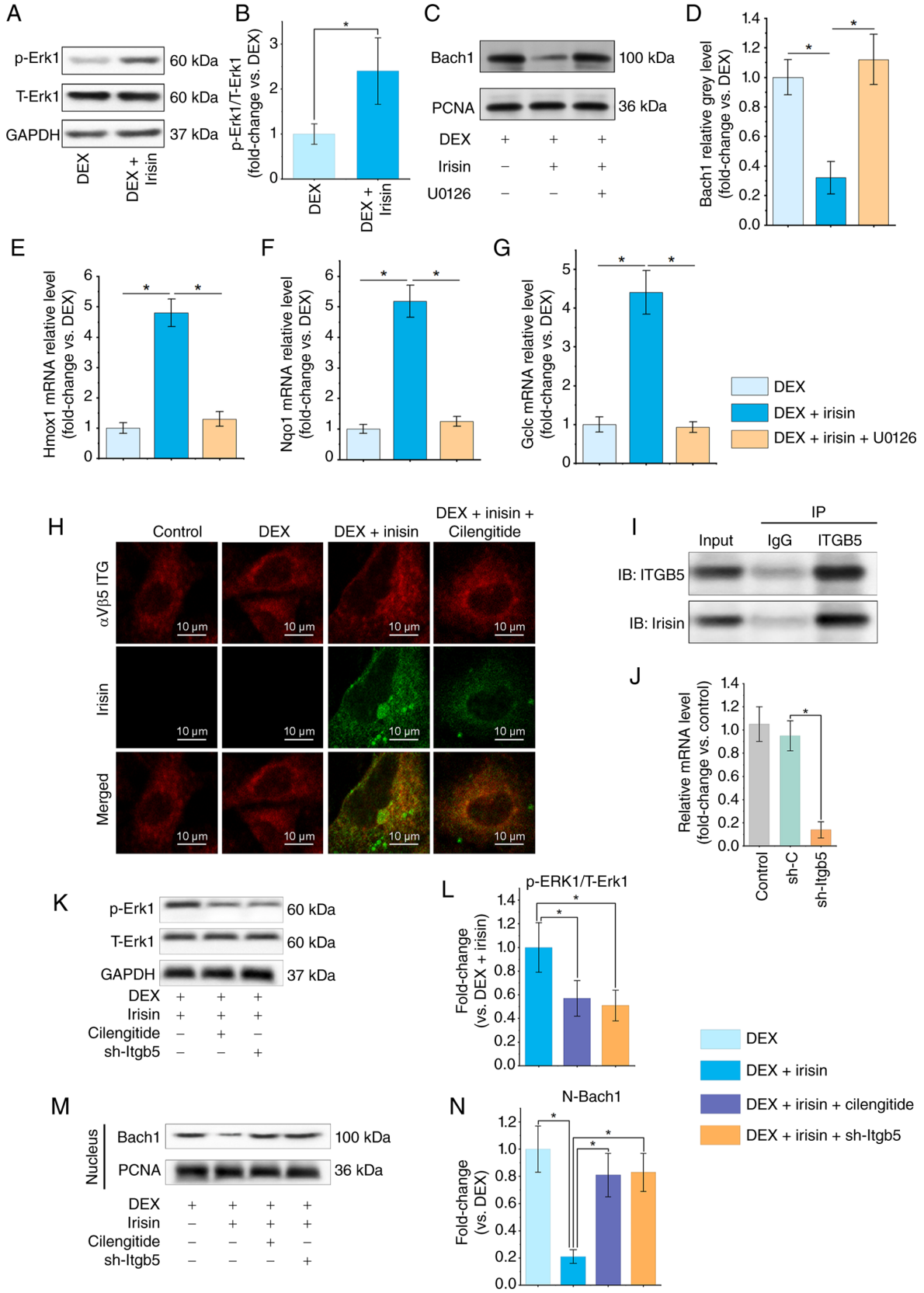


Figure 7. Irisin activates Erk1 signaling via ITG αVβ5 to promote Bach1 nuclear export. (A) Western blot analysis of p- and T-Erk1. (B) Quantification of p-Erk1/T-Erk1 ratio. (C) Western blot analysis of nuclear Bach1 levels. (D) Semi-quantification of nuclear Bach1. Relative mRNA expression levels of (E) Hmox1, (F) Nqo1 and (G) Gclc. (H) Immunofluorescence colocalization of irisin (green) and αVβ5 ITG (red). Nuclei were stained with DAPI (blue). Scale bar, 10 μm. (I) Co-IP analysis of the interaction between irisin and ITGB5. Whole-cell lysates were immunoprecipitated with anti-ITGB5 antibodies (normal IgG was used as a negative control), followed by immunoblotting for ITGB5 and irisin. (J) Relative mRNA levels of Itgb5 in Control, sh-C and sh-Itgb5 cells, as determined by reverse transcription-quantitative PCR. (K) Western blot analysis and semi-quantification (L) of p-/T-Erk1 in cells treated with cilengitide or sh-Itgb5. (M) Western blot analysis and (N) semi-quantification of nuclear Bach1. Data are presented as the mean ± SD. *P<0.05. DEX, dexamethasone; Gclc, glutamate-cysteine ligase catalytic subunit; Hmox1, heme oxygenase-1; IB, immunoblotting; IP, immunoprecipitation; ITG, integrin; Nqo1, NAD(P)H quinone oxidoreductase 1; p-, phosphorylation; PCNA, proliferating cell nuclear antigen; sh, short hairpin; sh-C, control shRNA; T-, total.

redox homeostasis (13). Studies have established that Bach1 inhibition protects osteoblasts against oxidative damage by enhancing Nrf2/ARE signaling activation, and that pharmacological Bach1 inhibition promotes nuclear export of Bach1 and induces Nrf2 nuclear accumulation (47,48). The present data demonstrated that irisin promoted nuclear export of Bach1, leading to decreased nuclear Bach1 levels and consequent relief of Nrf2 suppression. This conclusion is supported by two complementary lines of evidence: LMB, a CRM1 inhibitor, blocked irisin-induced Bach1 nuclear export and abrogated irisin-mediated protective effects; secondly, shRNA-mediated knockdown of Bach1 rendered LMB ineffective, demonstrating that the inhibitory effect of LMB was dependent on the presence of Bach1. These results established a causal role for Bach1 nuclear export in irisin-mediated Nrf2 activation.

The present study investigated the upstream signaling events governing irisin-induced Bach1 nuclear export. Irisin induced Erk1 phosphorylation in DEX-treated osteoblasts, whereas pharmacological inhibition of Erk1/2 with U0126 blocked both Bach1 nuclear export and irisin-induced cytoprotective effects, thereby establishing Erk1 as a requisite intermediate in this cascade. Accordingly, the present study aimed to identify the upstream receptor responsible for irisin-induced Erk1 activation. Accumulating evidence has identified ITG αVβ5 as a functional receptor for irisin in various cell contexts, including osteocytes, hippocampal neurons and vascular endothelial cells (24,48-50). Specifically, irisin has been shown to bind ITG αVβ5 and activate the Erk1/2 signaling pathway (51,52). Consistent with this, a recent study demonstrated that irisin signals via ITG αVβ5 to induce Erk1/2 phosphorylation and that pharmacological inhibition of αVβ5 with cilengitide effectively suppresses this activation (52). In the present study, co-IP and immunofluorescence co-localization confirmed the physical interaction between irisin and ITG αVβ5 in osteoblasts. Functional inhibition of ITG αVβ5 with cilengitide abrogated irisin-induced Erk1 phosphorylation and Bach1 nuclear export, and genetic knockdown of Itgb5 using shRNA produced similar effects, indicating that ITG αVβ5 may serve as the upstream receptor for irisin in osteoblasts. Collectively, these findings demonstrated a complete signaling cascade: Irisin bound ITG αVβ5, activated Erk1 phosphorylation, promoted nuclear export of Bach1, relieved Bach1-mediated suppression of Nrf2 and ultimately enhanced antioxidant gene expression to counteract oxidative stress and apoptosis.

The Nrf2 signaling pathway is a central hub in the protection against GC-induced ON and multiple therapeutic strategies converge on this axis (6,8,53). For example, Han *et al* (8) demonstrated that chlorogenic acid activated the Nrf2/HO-1 pathway via p21 upregulation to protect MC3T3-E1 cells from DEX-induced mitochondrial apoptosis. Similarly, Chen *et al* (53) reported that microRNA-3175 activated Nrf2 signaling by targeting DCAF1, thereby inhibiting DEX-induced oxidative injury in osteoblasts. The present findings extend these observations by identifying a novel upstream regulatory mechanism: Irisin promoted nuclear export of Bach1, a competitive suppressor of Nrf2, thereby relieving Nrf2 from transcriptional inhibition and enhancing antioxidant gene expression. This Bach1-centric mechanism distinguishes the present study from those that directly modulate Nrf2 stability or degradation and underscores the therapeutic potential of targeting the Bach1/Nrf2 axis as a complementary strategy for ONFH treatment.

Several limitations of the present study should be acknowledged. First, there was a species mismatch between the *in vivo* (Sprague-Dawley rats) and *in vitro* (murine MC3T3-E1 cells) experiments. Although this combination is common in preliminary investigations (54,55), it introduces potential inconsistencies in cross-species protein expression and antibody reactivity. Therefore, future studies employing rat-derived osteoblast cell lines are warranted to confirm the key findings. Additionally, the pharmacological tools used in the present study have inherent limitations. LMB is a general inhibitor of CRM1-mediated nuclear export rather than a Bach1-specific inhibitor and cilengitide inhibits multiple αV ITGs including αVβ3, αVβ5 and αVβ8 (56). Although the present study performed sh-Bach1 and sh-Itgb5 knockdown to genetically compensate for these limitations, future studies using specific inhibitors or blocking antibodies may validate the specificity of these interactions. Additionally, the present study did not directly verify whether U0126 alone affects baseline oxidative stress or apoptosis in control cells; therefore, future studies should include appropriate control experiments to exclude potential off-target effects of pharmacological inhibitors such as U0126. Moreover, the present study did not directly examine key signaling components of the proposed αVβ5/Erk1/Bach1/Nrf2 pathway, such as p-Erk1, nuclear Bach1 and nuclear Nrf2, in FH tissue. Future studies employing more advanced techniques, such as single-cell RNA sequencing or spatial transcriptomics, are warranted to delineate the cell type-specific activation of this pathway *in vivo*. Finally, the evidence for direct binding between irisin and ITG αVβ5, while strengthened by co-IP and sh-Itgb5 data, relied on functional and biochemical association rather than direct biophysical measurement. Future studies using surface plasmon resonance or biotin-labeled binding assays may clarify the direct binding kinetics.

Despite the aforementioned limitations, the present study provided evidence that irisin protected against GC-induced ONFH through the ITG αVβ5/Erk1/Bach1/Nrf2 signaling pathway. The present findings provide new insights into the molecular regulation of bone metabolism and redox homeostasis, and highlight the therapeutic potential of irisin for the prevention and treatment of ONFH. Future studies should focus on optimizing irisin delivery methods, evaluating its long-term safety and efficacy in preclinical models and translating these findings into clinical application.

Acknowledgements

Not applicable.

Funding

The present study was supported by Grants for National Natural Science Foundation of China (grant no. 81772355).

Availability of data and materials

The data generated in the present study may be requested from the corresponding author.

Authors' contributions

XZ conceptualized and designed the study, developed the methodology, performed the formal analysis, conducted the animal and cell experiments, and wrote the original draft of the manuscript. YuZ and YaZ performed the animal experiments, and the histological and molecular assays. KN participated in the establishment of the GC-induced ONFH animal model and in the acquisition of the experimental data, and acquired and analyzed the micro-CT and immunofluorescence data. KS and XL performed the co-IP and lentiviral knockdown experiments, and contributed to the analysis and interpretation of the data. LF conceptualized and supervised the study, acquired funding and revised the manuscript. All authors read and approved the final manuscript. XZ and LF confirm the authenticity of all the raw data.

Ethics approval and consent to participate

All animal care and experimental procedures were approved by the Laboratory Animal Ethics Committee of Xi'an Jiaotong University (Xi'an, China; approval no. XJTUAE2025-1953).

Patient consent for publication

Not applicable.

Competing interests

The authors declare that they have no competing interests.

References

1. Weinstein RS: Glucocorticoid-induced osteoporosis and osteonecrosis. Endocrinol Metab Clin North Am 41: 595-611, 2012.
2. Assouline-Dayan Y, Chang C, Greenspan A, Shoenfeld Y and Gershwin ME: Pathogenesis and natural history of osteonecrosis. Semin Arthritis Rheum 32: 94-124, 2002.
3. Mont MA, Jones LC and Hungerford DS: Nontraumatic osteonecrosis of the femoral head: Ten years later. J Bone Joint Surg Am 88: 1117-1132, 2006.
4. Deng S, Dai G, Chen S, Nie Z, Zhou J, Fang H and Peng H: Dexamethasone induces osteoblast apoptosis through ROS-PI3K/AKT/GSK3β signaling pathway. Biomed Pharmacother 110: 602-608, 2019.
5. Zhan J, Yan Z, Zhao M, Qi W, Lin J, Lin Z, Huang Y, Pan X and Xue X: Allicin inhibits osteoblast apoptosis and steroid-induced necrosis of femoral head progression by activating the PI3K/AKT pathway. Food Funct 11: 7830-7841, 2020.
6. Yang N, Sun H, Xue Y, Zhang W, Wang H, Tao H, Liang X, Li M, Xu Y, Chen L, *et al*: Inhibition of MAGL activates the Keap1/Nrf2 pathway to attenuate glucocorticoid-induced osteonecrosis of the femoral head. Clin Transl Med 11: e447, 2021.
7. Circu ML and Aw TY: Reactive oxygen species, cellular redox systems, and apoptosis. Free Radic Biol Med 48: 749-762, 2010.
8. Han D, Gu X, Gao J, Wang Z, Liu G, Barkema HW and Han B: Chlorogenic acid promotes the Nrf2/HO-1 anti-oxidative pathway by activating $p21^{Waf1/Cip1}$ to resist dexamethasone-induced apoptosis in osteoblastic cells. Free Radic Biol Med 137: 1-12, 2019.
9. Li J, Ge Z, Fan L and Wang K: Protective effects of molecular hydrogen on steroid-induced osteonecrosis in rabbits via reducing oxidative stress and apoptosis. BMC Musculoskelet Disord 18: 58, 2017.
10. Sun YX, Xu AH, Yang Y and Li J: Role of Nrf2 in bone metabolism. J Biomed Sci 22: 101, 2015.
11. Baird L and Yamamoto M: The molecular mechanisms regulating the KEAP1-NRF2 pathway. Mol Cell Biol 40: e00099-20, 2020.
12. Cai Y, Li B, Peng D, Wang X, Li P, Huang M, Xing H and Chen J: Crm1-dependent nuclear export of Bach1 is involved in the protective effect of hyperoside on oxidative damage in hepatocytes and CCl_4-induced acute liver injury. J Inflamm Res 14: 551-565, 2021.
13. Wang Y, Qiu J, Yan H, Zhang N, Gao S, Xu N, Wang C and Lou H: The Bach1/HO-1 pathway regulates oxidative stress and contributes to ferroptosis in doxorubicin-induced cardiomyopathy in H9c2 cells and mice. Arch Toxicol 98: 1781-1794, 2024.
14. Lignitto L, LeBoeuf SE, Homer H, Jiang S, Askenazi M, Karakousi TR, Pass HI, Bhutkar AJ, Tsirigos A, Ueberheide B, *et al*: Nrf2 activation promotes lung cancer metastasis by inhibiting the degradation of Bach1. Cell 178: 316-329. e18, 2019.
15. Nishizawa H, Yamanaka M and Igarashi K: Ferroptosis: Regulation by competition between NRF2 and BACH1 and propagation of the death signal. FEBS J 290: 1688-1704, 2023.
16. Wei X, He Y, Yu Y, Tang S, Liu R, Guo J, Jiang Q, Zhi X, Wang X and Meng D: The multifaceted roles of BACH1 in disease: Implications for biological functions and therapeutic applications. Adv Sci (Weinh) 12: e2412850, 2025.
17. Pedersen BK and Febbraio MA: Muscles, exercise and obesity: Skeletal muscle as a secretory organ. Nat Rev Endocrinol 8: 457-465, 2012.
18. Lan T, Yan X, Li J, Gu H, Hou Q, He E and Yang Q: Irisin, the myokine: Guardian and mediator in cardiovascular system. Endocrinol Diabetes Metab 8: e70097, 2025.
19. Xu L, Shen L, Yu X, Li P, Wang Q and Li C: Effects of irisin on osteoblast apoptosis and osteoporosis in postmenopausal osteoporosis rats through upregulating Nrf2 and inhibiting NLRP3 inflammasome. Exp Ther Med 19: 1084-1090, 2020.
20. Colaianni G, Cuscito C, Mongelli T, Oranger A, Mori G, Brunetti G, Colucci S, Cinti S and Grano M: Irisin enhances osteoblast differentiation in vitro. Int J Endocrinol 2014: 902186, 2014.
21. He Z, Li H, Han X, Zhou F, Du J, Yang Y, Xu Q, Zhang S, Zhang S, Zhao N, *et al*: Irisin inhibits osteocyte apoptosis by activating the Erk signaling pathway in vitro and attenuates ALCT-induced osteoarthritis in mice. Bone 141: 115573, 2020.
22. Storlino G, Colaianni G, Sanesi L, Lippo L, Brunetti G, Errede M, Colucci S, Passeri G and Grano M: Irisin prevents disuse-induced osteocyte apoptosis. J Bone Miner Res 35: 766-775, 2020.
23. Qiao X, Nie Y, Ma Y, Chen Y, Cheng R, Yin W, Hu Y, Xu W and Xu L: Irisin promotes osteoblast proliferation and differentiation via activating the MAP kinase signaling pathways. Sci Rep 6: 18732, 2016.
24. Ma Y, Qiao X, Zeng R, Cheng R, Zhang J, Luo Y, Nie Y, Hu Y, Yang Z, Zhang J, *et al*: Irisin promotes proliferation but inhibits differentiation in osteoclast precursor cells. FASEB J 32: 5813-5823, 2018.
25. Colaianni G, Cuscito C, Mongelli T, Pignataro P, Buccoliero C, Liu P, Lu P, Sartini L, Di Comite M, Mori G, *et al*: The myokine irisin increases cortical bone mass. Proc Natl Acad Sci USA 112: 12157-12162, 2015.
26. Zhang X, Hu C, Kong CY, Song P, Wu HM, Xu SC, Yuan YP, Deng W, Ma ZG and Tang QZ: FNDC5 alleviates oxidative stress and cardiomyocyte apoptosis in doxorubicin-induced cardiotoxicity via activating AKT. Cell Death Differ 27: 540-555, 2020.
27. Zhang M, Xu Y and Jiang L: Irisin attenuates oxidized low-density lipoprotein impaired angiogenesis through AKT/mTOR/S6K1/Nrf2 pathway. J Cell Physiol 234: 18951-18962, 2019.
28. Chen RR, Fan XH, Chen G, Zeng GW, Xue YG, Liu XT and Wang CY: Irisin attenuates angiotensin II-induced cardiac fibrosis via Nrf2 mediated inhibition of ROS/TGFβ1/Smad2/3 signaling axis. Chem Biol Interact 302: 11-21, 2019.
29. Du J, Fan X, Yang B, Chen Y, Liu KX and Zhou J: Irisin pretreatment ameliorates intestinal ischemia/reperfusion injury in mice through activation of the Nrf2 pathway. Int Immunopharmacol 73: 225-235, 2019.
30. Percie Du Sert N, Hurst V, Ahluwalia A, Alam S, Avey MT, Baker M, Browne WJ, Clark A, Cuthill IC, Dirnagl U, *et al*: The ARRIVE guidelines 2.0: Updated guidelines for reporting animal research. PLoS Biol 18: e3000410, 2020.
31. National Research Council: Guide for the Care and Use of Laboratory Animals. 8th edition. The National Academies Press, Washington, DC, 2011.

32. Okazaki S, Yamazaki E, Tamura K, Hoshiya T, Anabuki K, Tanaka H and Tanaka G: A 13-week subcutaneous toxicity study of prednisolone farnesylate (PNF) in rats. J Toxicol Sci 17 (Suppl 3): S1-S48, 1992 (In Japanese).
33. Tao SC, Yuan T, Rui BY, Zhu ZZ, Guo SC and Zhang CQ: Exosomes derived from human platelet-rich plasma prevent apoptosis induced by glucocorticoid-associated endoplasmic reticulum stress in rat osteonecrosis of the femoral head via the Akt/Bad/Bcl-2 signal pathway. Theranostics 7: 733-750, 2017.
34. Zhang J, Valverde P, Zhu X, Murray D, Wu Y, Yu L, Jiang H, Dard MM, Huang J, Xu Z, *et al*: Exercise-induced irisin in bone and systemic irisin administration reveal new regulatory mechanisms of bone metabolism. Bone Res 5: 16056, 2017.
35. American Veterinary Medical Association: AVMA Guidelines for the Euthanasia of Animals: 2020 edition. American Veterinary Medical Association, Schaumburg, IL, 2020.
36. Bouxsein ML, Boyd SK, Christiansen BA, Guldberg RE, Jepsen KJ and Müller R: Guidelines for assessment of bone microstructure in rodents using micro-computed tomography. J Bone Miner Res 25: 1468-1486, 2010.
37. Nan K, Zhang Y, Zhang X, Li D, Zhao Y, Jing Z, Liu K, Shang D, Geng Z, Fan L, *et al*: Exosomes from miRNA-378-modified adipose-derived stem cells prevent glucocorticoid-induced osteonecrosis of the femoral head by enhancing angiogenesis and osteogenesis via targeting miR-378 negatively regulated suppressor of fused (Sufu). Stem Cell Res Ther 12: 331, 2021.
38. Livak KJ and Schmittgen TD: Analysis of relative gene expression data using real-time quantitative PCR and the 2(-Delta Delta C(T)) method. Methods 25: 402-408, 2001.
39. Zhu XW, Ding K, Dai XY and Ling WQ: β-aminoisobutyric acid accelerates the proliferation and differentiation of MC3T3-E1 cells via moderate activation of ROS signaling. J Chin Med Assoc 81: 611-618, 2018.
40. Bi J, Zhang J, Ren Y, Du Z, Li T, Wang T, Zhang L, Wang M, Wu Z, Lv Y and Wu R: Irisin reverses intestinal epithelial barrier dysfunction during intestinal injury via binding to the integrin αVβ5 receptor. J Cell Mol Med 24: 996-1009, 2020.
41. Li X, Qian S, Chen D, Li ZZ, Chen KY, Pan YP, Lv XH, Jia RQ and Yu XF: A new mechanism in steroid-induced osteonecrosis of the femoral head and the protective role of simvastatin. Exp Cell Res 446: 114471, 2025.
42. Zhang X, Yang Z, Xu Q, Xu C, Shi W, Pang R, Zhang K, Liang X, Li H, Li Z and Zhang H: Dexamethasone induced osteocyte apoptosis in steroid-induced femoral head osteonecrosis through ROS-mediated oxidative stressOrthop Surg 16: 733-744, 2024.
43. Petek D, Hannouche D and Suva D: Osteonecrosis of the femoral head: Pathophysiology and current concepts of treatment. EFORT OPEN Rev 4: 85-97, 2019.
44. Zhu X, Li X, Wang X, Chen T, Tao F, Liu C, Tu Q, Shen G and Chen JJ: Irisin deficiency disturbs bone metabolism. J Cell Physiol 236: 664-676, 2021.
45. Hu X, Zhang H, Wang Z, Zhao X, Hu T, Liu C, Chen X, Wang W and Lu S: Exercise-derived irisin prevents bone loss via Nrf2 5 activation and inhibition of STING/NF-κB signaling. Free Radic Biol Med 246: 51-68, 2026.
46. Kim H, Wrann CD, Jedrychowski M, Vidoni S, Kitase Y, Nagano K, Zhou C, Chou J, Parkman VA, Novick SJ, *et al*: Irisin mediates effects on bone and fat via αv integrin receptors. Cell 175: 1756-1768.e17, 2018.
47. Wada S, Kanzaki H, Katsumata Y, Yamaguchi Y, Narimiya T, Attucks OC, Nakamura Y and Tomonari H: Bach1 inhibition suppresses osteoclastogenesis via reduction of the signaling via reactive oxygen species by reinforced antioxidation. Front Cell Dev Biol 8: 740, 2020.
48. Tian X, Cong F, Guo H, Fan J, Chao G and Song T: Downregulation of Bach1 protects osteoblasts against hydrogen peroxide-induced oxidative damage in vitro by enhancing the activation of Nrf2/ARE signaling. Chem Biol Interact 309: 108706, 2019.
49. Ma M, Tian Y, Yin R, Jing G and Zhang M: FNDC5/irisin ameliorates diabetes-associated cognitive dysfunction via αVβ5-cAMP signaling to regulate oxidative stress, neuroinflammation and synaptic plasticity. J Transl Med 24: 642, 2026.
50. A M, Wales TE, Zhou H, Draga-Coletă SV, Gorgulla C, Blackmore KA, Mittenbühler MJ, Kim CR, Bogoslavski D, Zhang Q, *et al*: Irisin acts through its integrin receptor in a two-step process involving extracellular Hsp90α. Mol Cell 83: 1903-1920.e12, 2023.
51. Fang L, Li W, Zhao H, Wang W, Gao H, Wang P, Zhang X, Lv R, Xu F, Chen J, *et al*: Irisin alleviates steroid-induced vascular dysfunction by regulating the αVβ5-c-Abl-Caveolin-1 signaling pathway. Biochem Pharmacol 236: 116870, 2025.
52. Tan A, Li T, Yang J, Li X, Li W and Yu J: Irisin regulates integrin αvβ5/FAK/ERK to inhibit neutrophil extracellular traps formation and reduce pancreatic beta-cells pyroptosis in type 2 diabetes mellitus. Diabetol Metab Syndr 17: 279, 2025.
53. Chen J, Liang J, Zhen YF, Chang L, Zhou Z and Shen X: DCAF1-targeting microRNA-3175 activates Nrf2 signaling and inhibits dexamethasone-induced oxidative injury in human osteoblasts. Cell Death Dis 12: 1024, 2021.
54. Lin J, Zhang R, Lin X, Luo X, Lin H, Xu J and Lin S: Oleuropein attenuates steroid-induced osteonecrosis of the femoral head by inhibiting osteoblast apoptosis via activation of the PI3K-AKT-Bcl2 pathway. Sci Rep 16: 21071, 2026.
55. Chen Q, Wang B, Liang H, Xu H, Zhang K and Hao Y: Bilobalide attenuates steroid-induced osteonecrosis of the femoral head by upregulating the ERK/HIF-1α signaling pathway and promoting angiogenesis-osteogenesis coupling. Sci Rep 16: 7755, 2026.
56. Kudo N, Matsumori N, Taoka H, Fujiwara D, Schreiner EP, Wolff B, Yoshida M and Horinouchi S: Leptomycin B inactivates CRM1/exportin 1 by covalent modification at a cysteine residue in the central conserved region. Proc Natl Acad Sci USA 96: 9112-9117, 1999.

Copyright © 2026 Zhang et al. This work is licensed under a Creative Commons Attribution-NonCommercial-NoDerivatives 4.0 International (CC BY-NC-ND 4.0) License.